Load Analysis of Ankle Foot Orthoses during Gait

by

Atichart Kwanyuang

Department of Bioengineering

University of Strathclyde

Glasgow

2012

This thesis is submitted in partial fulfillment of the requirements for Master of Science in Bioengineering

This thesis is the result of the author's original research. It has been composed by the author and has not been previously submitted for examination which has led to the award of a degree.

Signed:

Date:

Abstract

Different causes of gait deficiencies generate different symptoms. It is important for orthotists to gain a better understanding on how to design Ankle Foot Orthoses (AFOs) in order to address individual biomechanical requirements. The loads acting on AFOs during gait are important factors for orthotists to accurately understand so as to design AFOs more effectively. Therefore, the aim of this study is to develop a validated Finite Element (FE) model, which could be used to quantify and analyse the loads acting on an AFO during gait. In this thesis, for mutual comparison and confirmation, pressures acting on the AFO are recorded by two different types of pressure transducers: resistive and capacitive. Trends of the results obtained from the two sensors are similar; however, the magnitudes tend to be different. Furthermore, an accurate digital 3D scanning model of an AFO is captured using the 3D digitiser which can be modified by Computer Aided Design (CAD) software before being exported to Finite Element Analysis (FEA) software to create an FE model. Both the loads measured from the experiment and the assumed constraint during heel off are then applied to the FE model. To make the analysis more complete, a number of features of AFO and a range of FEA methods are conducted. The results are validated by both empirical findings from previous literature and an additional experiment carried out. Based on a healthy subject with no pathological gait, this study reveals that, on the one hand, the AFO is able to assist walking by carrying 6.89% of the overall magnitude of ground reaction force. On the other hand, it resists walking by generating 18.63% in dorsiflexion of the overall magnitude of the moment generated by the plantarflexors. It is therefore claimed that these findings are useful for orthotists involved in fitting AFOs, in order to efficiently design and construct them.

Acknowledgements

My greatest gratitude and appreciation goes to my supervisor Stephanos Solomonidis for his valuable advice, expertise, and endless encouragement. I would like to thank John Maclean his technical support and Stephen Murray for his help with using his facilities. I would also like to extend my appreciation to Enrica Papi for providing a result of her tensile test and Anthony Crimin for his help in collecting data using Vicon.

I would like to thank Nicola Cairns and Duncan Lindsay for their help with using the DMEM facilities. I would also like to thank Arjan Buis for his help using his Tekscan equipment and Daniel Rafferty for his help using his novel equipment. My gratitude and appreciation goes to Scott Telfer for his help in collecting data using pedar and Thanapol Luckanawat for his advice on FEA.

I am extremely grateful to the Royal Thai Government for providing funding for my MSc.

My greatest gratitude and appreciation also goes to my subject for being a willing volunteer.

This thesis would never have been completed without the encouragement and devotion of my family and friends.

Table of Contents

Abstract ii

Acknowledgements iii

List of Figures vi

List of Tables viii

Chapter 1 Introduction 1

1.1 Background 1

1.2 Aims and objectives 3

1.3 Layout of thesis 4

Chapter 2 Literature review 5

2.1 Introduction 5

2.2 Measurement of the practical loads on the AFOs 5

2.3 Measurement of the theoretical loads on the AFOs 8

Chapter 3 Pressure measurement experiments 11

3.1 Introduction to pressure measurement experiments 11

3.2 Methodology and instrumentation 11

3.2.1 F-Scan system experiment 11

3.2.2 Data analysis of F-Scan system experiment 14

3.2.3 pedar system experiment 19

3.2.4 Data analysis of pedar system experiment 20

3.3 Results 22

3.3.1 F-Scan system experiment 22

3.3.2 pedar system experiment 26

3.3.3 Comparison between F-Scan and pedar system 28

3.4 Discussion 30

Chapter 4 3D scanning 35

4.1 Introduction to 3D scanning 35
4.2 Methodology and instrumentation 35
4.3 Results 39
4.4 Discussion 41
Chapter 5 Finite element analysis 43
5.1 Introduction to finite element analysis 43
5.2 Methodology and instrumentation 43
5.2.1 Geometry 44
5.2.2 Mesh 49
5.2.3 Static structural analysis 50
5.2.4 Validation 60
5.3 Results 63
5.4 Discussion 67
Chapter 6 Conclusion 71
6.1 General conclusions 71
6.2 Recommendations for further study 72
References 73

List of Figures

Figure 3-1 The F-Scan system sensor equilibration and calibration set up: (1) laptop computer with F-Scan software, (2) PCI expansion, (3) cuff unit, (4) sensor model 9811, (5) equilibrator, (6) pressure regulator with pressure gauge 12
Figure 3-2 Sensor positions: (1) sole, (2) central calf, (3) lateral calf, (4) medial calf, (5) ankle, (6) strap 13
Figure 3-3 The AFO with F-Scan system set up worn by the subject 14
Figure 3-4 A plot of plantar force versus frames.....15
Figure 3-5 Four components in the gait cycle that were analysed 15
Figure 3-6 (a) plantar sensor split into six sections and (b) central calf sensor split into three sections for analysis using F-Scan Research software.....16
Figure 3-7 Pressure measurement at central calf position without EVA foam sheet applied.....17
Figure 3-8 Pressure measurement at central calf position with three-ply EVA foam sheet applied 18
Figure 3-9 EVA foam sheet applying on the sensor at the defective positions.....18
Figure 3-10 pedar®-x system: (1) pedar®-x insole, (2) Bluetooth™ telemetry system, (3) rechargeable NiMH battery.....19
Figure 3-11 pedar®-x Expert software 20
Figure 3-12 Plot of plantar force collected from the pedar system experiment versus time.....21
Figure 3-13 Peak contact pressure measured by each sensor throughout the test and sensors divided into sections similar to model 3000 sensor 22
Figure 3-14 Plot of maximum pressure measured by model 3000 sensor during gait 23
Figure 3-15 Plot of average pressure measured by model 3000 sensor during gait 23
Figure 3-16 Plot of maximum pressure versus frames using F-Scan Research software.....24
Figure 3-17 Plot of maximum pressure measured by model 9811 sensor during gait 25
Figure 3-18 Plot of average pressure measured by model 9811 sensor during gait 25
Figure 3-19 The unknown error that the pressure measured shown in the plot (1) does not correspond to the pressure measured shown in the sensor map (2) 26

Figure 3-20 Plot of maximum pressure measured by pedar®-x insole during gait....27
Figure 3-21 Plot of average pressure measured by pedar®-x insole during gait 27
Figure 3-22 Plot of average pressure measured by both systems during foot flat ...28
Figure 3-23 Plot of average pressure measured by both systems during midstance 29
Figure 3-24 Plot of average pressure measured by both systems during heel off ...30
Figure 4-1 Homopolymer polypropylene AFO made by NCPO 36
Figure 4-2 (a) powder sprayed on AFO surface and (b) Ardrox 9D1B.....37
Figure 4-3 AFO and 3D digitiser set up for scanning.....37
Figure 4-4 Scanned data collected from 3D digitiser in Polygon Editing Tool software 39
Figure 4-5 Five steps of scanned data improvement in Geomagic software.....40
Figure 4-6 Complete Parasolid file acquired from NX software 41
Figure 4-7 Rough scanned data scanning on AFO surface without powder sprayed 42
Figure 5-1 Plot of stress-strain data gained from homopolymer polypropylene 200-cycle tensile test done by Enrica Papi.....44
Figure 5-2 Young's modulus quantified from the gradient of the 30th cycle stress-strain curve.....45
Figure 5-3 Thickness gauge modification.....46
Figure 5-4 The AFO thickness measurement set up 46
Figure 5-5 33 positions of the AFO thickness measurement 47
Figure 5-6 AFO split in to eight thickness regions 48
Figure 5-7 Locations of loads applied on FE model of AFO 51
Figure 5-8 Directions and magnitudes of pressures applied on FE model of AFO...52
Figure 5-9 A plot of lower strap force versus frames 53
Figure 5-10 Sensor positions: (1) sole, (2) strap 53
Figure 5-11 A plot of upper strap force versus frames.....54
Figure 5-12 Plot of strap force measured by model 9811 sensor during gait.....54
Figure 5-13 Directions and magnitudes of forces applied on FE model of AFO.....55
Figure 5-14 Two possible areas to apply constraint in FEA.....56
Figure 5-15 The images defined in term of gait components.....57
Figure 5-16 The simulation in analysis number 12 validated the image represented heel off.....58

Figure 5-17 The simulation in analysis number 8 validated the image represented heel off....58
Figure 5-18 Strain probe position....60
Figure 5-19 Homopolymer polrpropylene AFO with 45° rectangular single-plane rosette strain gauge (a) installed in posterior ankle region at 75.00mm in height from the bottom surface....61
Figure 5-20 Plot of calculated strain data against time....62
Figure 5-21 Plot of calculated strain data against time in one gait cycle shows the tensile strain generated during heel off....63
Figure 5-22 Graphics image of von Mises stress distribution in AFO in analysis number 8....65
Figure 5-23 Graphics image of von Mises stress distribution in AFO in analysis number 13....65

List of Tables

Table 5-1 The AFO thickness measurement results with the average thickness and the standard deviation....47
Table 5-2 Average AFO thickness in each region....48
Table 5-3 The analysis results of mesh sensitivity study....50
Table 5-4 The details of four analyses....59
Table 5-5 The results of four analyses....64

Chapter 1 Introduction

1.1 Background

An orthosis is a mechanical appliance or apparatus that imposes counter forces on a limb in order to support it, to prevent or correct deformities, or to impart active function to a part of the limb. There are four functional classes of orthosis: 1) stabilisation or supportive, 2) motorised, 3) functional and corrective, and 4) protective. This is a definition of the orthosis defined in an orthopaedic dictionary (Hoppenfeld and Zeide 1994). Correspondingly, the International organization for standardization (ISO) established nine basic objectives to define the clinical objectives of the orthotic treatment identified as follows:

- To relieve pain
- To manage deformities
- To prevent an excessive range of joint motion
- To increase the range of joint motion
- To compensate for abnormalities of segment length or shape
- To manage abnormal neuromuscular function (e.g. weakness or hyperactivity)
- To protect tissues
- To promote healing
- To provide other effects (e.g. placebo, warmth, postural feedback).

The final segment of the standard described the functional requirements of the orthosis necessary to achieve the defined clinical objectives listed as follows:

- To prevent, reduce, or stabilize a deformity
- To modify the range of motion of a joint
- To add to the length or alter the shape of a segment
- To compensate for weak muscle activity or control muscle hyperactivity
- To reduce or redistribute the load on tissues.

The orthosis can be rationally and succinctly prescribed by specifying the desired functional outcome in biomechanical terms. A lower limb orthosis is among the most commonly prescribed biomechanical devices intended to assist individuals with

neuromuscular deficits (Henderson and Lamoreux 1969; ISO 2003; Hsu, Michael et al. 2008).

An ankle foot orthosis (AFO) used to control the alignment and motion of the foot and the ankle and thereby affect the entire body for individuals who need ankle control. Moreover, the AFO may enable the patients to achieve the same functional goals as would be possible with knee ankle foot orthosis (KAFO) and higher orthosis (Edelstein and Bruckner 2002). For patients with musculoskeletal or neuromuscular dysfunction, the AFO can be prescribed to accomplish various goals. The AFO can be used to support the feet and ankles, maintain optimal functional alignment during activity, or limit motion to protect healing structures for patients with unstable ankles, whether from muscular imbalance or injury. The AFO can substitute for inadequate muscle function during key points in the gait cycle, optimize alignment and help to manage abnormal tone, or minimize the risk of deformity (e.g. equinovarus) associated with long-term hypertonicity for patients with neuromotor dysfunction such as cerebral palsy or after stroke (Ounpuu, Bell et al. 1996; Radtka, Skinner et al. 1997; Burtner, Woollacott et al. 1999; Chen, Yeung et al. 1999; Tyson and Thornton 2001; Gök, Küçükdeveci et al. 2003; Leung and Moseley 2003; de Wit, Buurke et al. 2004; Balaban, rol et al. 2007; Lucareli, Lima et al. 2007; Lusardi and Nielsen 2007; Bregman, De Groot et al. 2010).

Early 20th century, the orthoses were constructed primarily of metal, leather, and fabric. In the last 60 years, however, new plastics have led to revolutionary advancements in the profession, permitting increased durability and strength, and significant cosmetic improvements suitable for use in the construction of orthoses. One of the most important production-related characteristics of an orthotic material is its ability to be molded over a positive model. Because plastics can be readily formed, they are a very popular, widely used material for orthoses(Ofir and Sell 1980; Shamp 1983; Lusardi and Nielsen 2007).

The fabrication process begins once a prescription for a custom orthosis has been created. The traditional fabrication process is composed of six steps: making accurate measurements of the limb, taking a negative cast, creating three-dimensional positive model of the limb, modifying to incorporate the desired controls, creating the orthosis around the positive model, and fitting of the device to the patient (Lusardi and Nielsen 2007).

There are several studies (Yamamoto, Miyazaki et al. 1993; Chu and Feng 1998; Bregman, De Groot et al. 2010) reported a lack of information to aid the orthotist in the efficient design and fabrication of the AFOs. There are a few experiments quantifying the biomechanical characteristics of AFOs available in the scientific literature. The precise knowledge of the loads acting on the AFO can be helpful for the orthotist to design the AFO to match the functional needs of the patient.

Because the biomechanical characteristics of each AFO can be usually discovered after it was made, this is rarely possible to modify its design to improve the biomechanical characteristics except to build a new one. Using of computer-aided design (CAD) together with finite element analysis (FEA) will allow the orthotist to develop the AFO to meet the biomechanical requirements before fabrication. Flexibility of design, speed of production, and consistency of quality and standardisation are potential advantages of using computer to aid orthotist to design the AFO (Lord and Jones 1988). Several studies (Leone, Diemente et al. 1988; Chu, Reddy et al. 1995; Syngellakis, Arnold et al. 2000) attempted to develop a finite element (FE) model of the AFO to quantify its biomechanical characteristics, however, the simulation results were rarely validated by any real-world experiments. Consequently, the validity of their findings has never been verified.

1.2 Aims and objectives

To have a better understanding of the loads applying on the AFO and to use CAD together with FEA to quantify the biomechanical characteristics aid to improve the design of the AFO before construction are potentially useful for the orthotist. As well as an awareness of the limitations of the real-world experiment and the FEA of the AFO studies to date, the aim of this study is to develop a validated FE model of an AFO which can be used to analyse the loads applied during gait.

This aim is achieved through the specific objectives identified as follows:

- To measure the pressures acting on an AFO during normal gait using two different pressure measurement systems
- To calculate the position and magnitude of the pressures acting on the AFO using the experimental data

- To make an accurate 3D digital surface model of the AFO using 3D digitiser together with CAD software for further analysis
- To develop an FE model of the AFO and to predict the stresses, strains, and loads acting on the AFO using FEA software
- To validate the FEA results using experimental strain data from a corresponding real-world experiment
- To analyse the stresses, strains, and loads acting on the AFO using the FEA results.

1.3 Layout of thesis

First, chapter 2 presents a literature review corresponding to a study in this thesis. The detail of two different pressure measurement experiments is explained, and their results are then analysed and discussed in chapter 3. Next, chapter 4 clarifies a 3D scanning process of the AFO and a 3D model preparation for further analysis with FEA software. The data from the two previous chapters is used to develop an FE model for an FEA, and the results from the FEA are then analysed, validated, and discussed in chapter 5. Finally, Chapter 6 concludes the thesis by summarizing what was done and making recommendations for further studies.

Chapter 2 Literature review

2.1 Introduction

Although there are several studies involved with the AFOs, only a few studies quantified the biomechanical characteristics of the AFOs. Almost all of studies focused on determining the clinical characteristics of the AFOs. In like manner, several studies reported a lack of knowledge in biomechanical properties of the AFOs supporting the efficient AFOs development (Yamamoto, Miyazaki et al. 1993; Chu, Reddy et al. 1995; Bregman, Rozumalski et al. 2009). Therefore, this review is not much in length as it should be.

There are two sections in this review, one section clarifies the studies involved with using of practical methods to determine loads acting on the AFOs during gait, and another one explains the studies investigating loads acting on the AFOs using of FEA software.

2.2 Measurement of the practical loads on the AFOs

A study by Robin et al. performed experiments placing strain gauges in different types of below-knee drop-foot braces to measure various stresses applied on braces and to determine effects of various gait patterns on braces for mechanical improvement in standard designs of braces. The strain gauges were attached in different position that considered the area of the maximum stress probably generated depended on types of braces. The subject in this study was a healthy adult with no any pathological gait. In posterior spring braces, the strain gauges experienced the maximum tensile stress during swing phase that could shorten life of braces. To improve the design mechanically, either inserting mechanism used to reduce the tensile effects of gravity, or using less-rigid materials would be done. In both of single and double lateral upright braces, the strain gauges experienced significantly lower stresses than posterior spring braces. The highest stresses were measured during heel-strike in the unilateral upright braces, while they were noticed during mid-stance in the bilateral upright braces. This was considered the difference might be related to inaccurate alignment of the brace joints. To improve the design of the two lateral upright braces, either using much lighter materials, or adding joint

at sub-talar level to reduce lateral brace rigidity would be performed (Robin, Magora et al. 1968).

A study by Chu et al. performed experiments to analyse stress on various types and various materials of custom-made AFOs to improve their design parameters. Five AFOs used in these experiments were flex, moderate, solid, standard, and varus AFOs. Eight biaxial rosette pattern strain gauges were attached to the specific locations along the lateral, middle, and medial areas of the lower neck of each AFO to measure a vertical and horizontal deformation simultaneously. The positive strain output represents the tensile stress and the negative strain output represents the compressive stress. The AFOs were applied by approximate 170lbs load and tested in ten motions both of stance and swing phase. The stresses measured were either compressive or tensile stresses depended on bending during motions. In slow forward walk, high compressive and tensile stresses were generated during both heel-strike and toe-off. The compressive and the tensile stresses were the maximum stress produced during heel-strike and toe-off respectively. For the moderate and solid AFOs, the tensile and the compressive peak stresses were located at the upper-neck, lateral, and medial areas. For the varus AFO, both of peak stresses were located at upper-neck and lateral areas. For the flex and standard AFOs, the tensile peak stress was located at the neck and lateral areas, while the compressive peak stress was located at neck and lateral areas of the flex AFO different from the standard AFO that this stress located at the neck area only. These could be shown the shear failure in the flex AFOs and confirmed the similarity in clinical observation. In other motions, dorsiflexion and plantarflexion, could be clearly clarified that the magnitude of the peak stresses depended on the width of the necks. The narrower the neck been, the higher the stress generated. In abduction and adduction found a major effect on the lateral side arc edge of the AFOs. The findings from these experiments could be clearly defined that the magnitude and the location of the stress concentration depended on the geometry of AFOs, different patients, and different activities. These experimental data were useful for the AFOs failure predictions (Chu and Feng 1998).

A study by Svensson et al. performed experiments mounting four strain gauges on a solid light weight carbon AFO at 60mm above the AFO sole to obtain the strain data in sagittal plane. Two strain gauges were attached in the medial side of AFO one at anterior and another one at posterior position, another two strain gauges were

attached in the lateral side of AFO at the corresponding positions. The strain characteristics were then changed when AFO moving in the ankle angle. Therefore, the strain information could be used to detect the inclination and to determine the inclination angle when walking. The experiments were performed on one healthy man walking continuously at various speeds and inclinations. The four strain sensor signals combined into one using a full Wheatstone bridge was the result of this experiment. The resulting strain sensor signal increased during plantarflexion, and decreased during dorsiflexion. In horizontal walking, the resulting signal increased during heel strike, and reached the maximum plantarflexion when the opposite foot lifted. The resulting signal decreased when the trunk moved forward until reached to zero when the trunk was above the ankle during midstance. The trunk continuous forwarded as well as the resulting signal continuous decreased showed the negative strain signal, abrupt decreasing occurred during heel rise, and reached the maximum dorsiflexion during push off. The resulting signal was then increased during late stance, and nearly reached a plateau at approximate zero during swing phase. In up hill walking, the heel strike phase was shorter than the heel strike phase in horizontal walking, while, in down hill walking, there was no difference compared to horizontal walking. As can be seen, the resulting signal could be used to detect the ankle angle of the AFO useful for gait analysis (Svensson, Salomonsson et al. 2007; Svensson and Holmberg 2010).

A study by Bregman et al. designed and developed a new device called BRUCE, Bi-articular Reciprocating Universal Compliance Estimator, to quantify the AFO characteristics, stiffness and neutral angle, that determine the function of the AFO in pathological gait. In this study, the moment around the ankle joint applied by the AFO per degree of ankle joint rotation used to define the stiffness of AFO ankle. To perform the experiment, the AFO was mounted into the device, either plantarflexion-dorsalflexion motion was then applied to deform the AFO at ankle within an interval ranging from 10° plantarflexion to 20° dorsalflexion, or flexion-extension motion was then applied to deform the AFO at metatarsal-phalangeal (MTP) within an interval ranging 0°-30° flexion. Software used to display the data measured by the force sensors was developed based on MATLAB software, and the result, the relationship between AFO ankle angle and moment, was determined by a linear model. Four AFOs: two different stiffness carbon-composite posterior leaf spring AFOs, one rigid polypropylene AFO, and one polypropylene posterior leaf spring AFO were used to test in this study. The tested results demonstrate that there is only one rigid

polypropylene AFO shows non-linear behavior due to buckling of the lateral side in ankle area, and the ankle stiffness was significantly higher than the MTP stiffness. This study can be useful to realize the role of biomechanical characteristics in correcting pathological gait (Bregman, Rozumalski et al. 2009).

2.3 Measurement of the theoretical loads on the AFOs

Two studies by Chu et al. developed an asymmetric three dimensional model of a polypropylene AFO and ankle-foot complex using computer aided design (CAD) software PATRAN. Both of three dimensional models consist of 596 nodes and 323 elements: 313 three dimensional solid elements (AFO, soft tissues, bones) and 10 three dimensional truss elements (ligaments) were then analysed using finite element analysis (FEA) software ADINA. Static analyses of the polypropylene AFO together with ankle-foot complex under normal and pathological conditions during gait were performed in this software to determine the distribution of stress in the AFO to answer the hypothesis that the maximum peak stress should occur in the neck and heel region of the AFO. The mechanical and material properties of the polypropylene AFO, soft tissues, bones, and ligaments were assumed to be isotropic, linear, and elastic. The upper boundary of the model of the AFO constrained to the model of the leg represents the AFO attached to the leg via strap in real situation. There was no leg motion considered in this analysis due to the upper boundary of the model of the leg was constrained in all axes. The model of the foot was constrained to the model of the leg as well. However, this constraint allows the model of the foot to move freely relative to the model of the leg. This analysis was assumed to be no slip between the model of the foot bones and the model of the soft tissues, and between the model of the soft tissues and the model of the AFO. The model of the tibia was connected to the model of the foot via the model of the ligaments, and could move vertically in the surrounding model of the soft tissues. The weight of the model of the foot was calculated by the mass proportional loading conditions. The forces applied in tendons and muscles, and the ground reaction forces during heel strike and toe off were simulated by concentrated nodal forces. The analysis results demonstrated that a high compressive stress was generated in the center of the heel region of the AFO during heel strike, and a high tensile stress was generated in the middle lateral neck region of the AFO during toe-off. During swing phase, the maximum compressive stress was located at the lateral

edge of the neck of the AFO, and the maximum tensile stress was detected at the medial side arc edge of the AFO. Additionally, the plantarflexion generated a high compressive stress in the central heel region, and a high tensile stress in the inner medial side arc edge of the AFO. The inversion produced the highest magnitude of compressive stress in the medial neck region of the AFO. The eversion produced a high compressive stress in the lateral neck region, and a high tensile stress in the inner side arc edge of the AFO. To sum up, the hypothesis can be confirmed by the results that the maximum peak stress occurred in the neck and heel regions of the AFO (Chu and Reddy 1995; Chu, Reddy et al. 1995).

A study of Syngellakis et al. developed a surface model of an AFO based on a number of lateral and anterior cross section profiles of a normal human right lower limb using finite element analysis (FEA) software ANSYS to determine the relationship between the trimline location and stiffness of the AFO for moderate and large rotations. A mesh consisting of 1708 nodes and 549 elements was then generated on the model of the AFO with a 2mm constant thickness throughout by automatic meshing in ANSYS software using the eight-node quadratic shell element type that has six degrees of freedom per node. A material used for AFO in this analysis is a copolymer polypropylene that its stress-strain relationship is non-linear above the glass transition temperature -20°C. The Young's modulus 1000MPa and 1390MPa were chosen to use in linear and non-linear analysis respectively. 0.35 was the Poisson's ratio choosing for the copolymer polypropylene using in this analysis. The constraints were applied in posterior areas of proximal calf region to fix the movement in anteroposterior axis, and in the heel to eliminate the movement in mediolateral axis. To investigate the effect of geometric non-linearity, a large deformation option was necessary to allow software to solve non-linear problem using Newton-Raphson method. To examine the effect of material non-linearity, the initial gradient of the non-linear stress-strain curve 1390MPa was used in this analysis instead of Young's modulus value 1000MPa quoted in the technical literature. This study also investigated the effect of combined non-linearity using the large deformation option together with multilinear elasticity. Moreover, two types of thickness: uniform and variable thicknesses were used in this analysis, and their results also compared to examine the effect of thickness. The results indicated that the simulated data using geometric non-linear analysis greater than the data obtained from linear analysis in plantar flexion, while smaller in dorsiflexion. Almost all of simulated data using material non-linear analysis very close to the data gained

from linear analysis in both plantar flexion and dorsiflexion. Almost all of simulated data using combined non-linear analysis greater than the data obtained from linear analysis in plantar flexion, but smaller in dorsiflexion. Almost all of simulated data between uniform and variable thickness were different that could be defined that variable thickness might have significant effect on the analysed data. Subsequently, the analyses were modified corresponding to the experiments performed by Sumiya et al. that evaluate the effect of ankle trimline of posterior-type plastic AFOs on stiffness control to validate the practical results (Sumiya, Suzuki et al. 1996; Sumiya, Suzuki et al. 1996). A comparison between analytical and experimental data for the resisting moment showed the similarity of both results indicated that the reliable and effective information could be obtained from the FEA software (Syngellakis, Arnold et al. 2000).

Chapter 3 Pressure measurement experiments

3.1 Introduction to pressure measurement experiments

The pressures applied on the AFO acting by lower limb would be considered to measure to quantify the accurate loading conditions occurring during the gait cycle. The reliable pressure measuring system was needed. In this study, two different types of pressure measuring system were selected to perform the tests. One was a resistive sensor (Kalamdani 2006) using electrical resistance to determine the pressure quantity called Tekscan pressure sensor (Tekscan Inc, Massachusetts, USA). The Tekscan pressure sensor is a thin multi-laminate construction consists of a large number of smaller sensing elements called sensels. Two models of Tekscan pressure sensor used in this study were model 3000 and 9811 for measurement in plantar area and other area in AFO respectively. Due to these sensors need F-Scan Research software to process the pressure data and the model 3000 is generally called the F-Scan sensor as well, the Tekscan pressure sensors were then called F-Scan system in this study. Another type using capacitive sensor technology to assess dynamic pressure distribution was pedar®-x insole (Novel GmbH, Germany) using together with Bluetooth™ telemetry and pedar®-x software, this system called pedar®-x system or pedar system in this study. The methodology and instrumentation, data analysis, and results of the two systems are explained individually, however, the two systems are also compared at the end of the result section.

3.2 Methodology and instrumentation

3.2.1 F-Scan system experiment

According to the F-Scan user manual, the F-Scan system needs an equilibration and calibration before using for pressure data collection. The equilibrator that has an internal bladder filling with air to apply a uniform pressure to the sensor pad was needed. The sensel area of each sensor was inserted into the equilibrator, and performed equilibration and calibration individually. The equilibration and calibration pressure was 200kPa controlled by pressure regulator (Fairchild Industrial Product Company, North Carolina, USA) inserting into the equilibrator. The sensor tab

extended outside of the equilibrator was inserted into a handle called cuff unit to gather and process the data from sensor before send to the computer. The cuff unit was connected to PCI expansion (Magma, California, USA) wiring to the laptop computer which F-Scan Research software already exists via PCI slot. Subsequently, the sensor could be equilibrated and calibrated by the F-scan software (Figure 3-1).

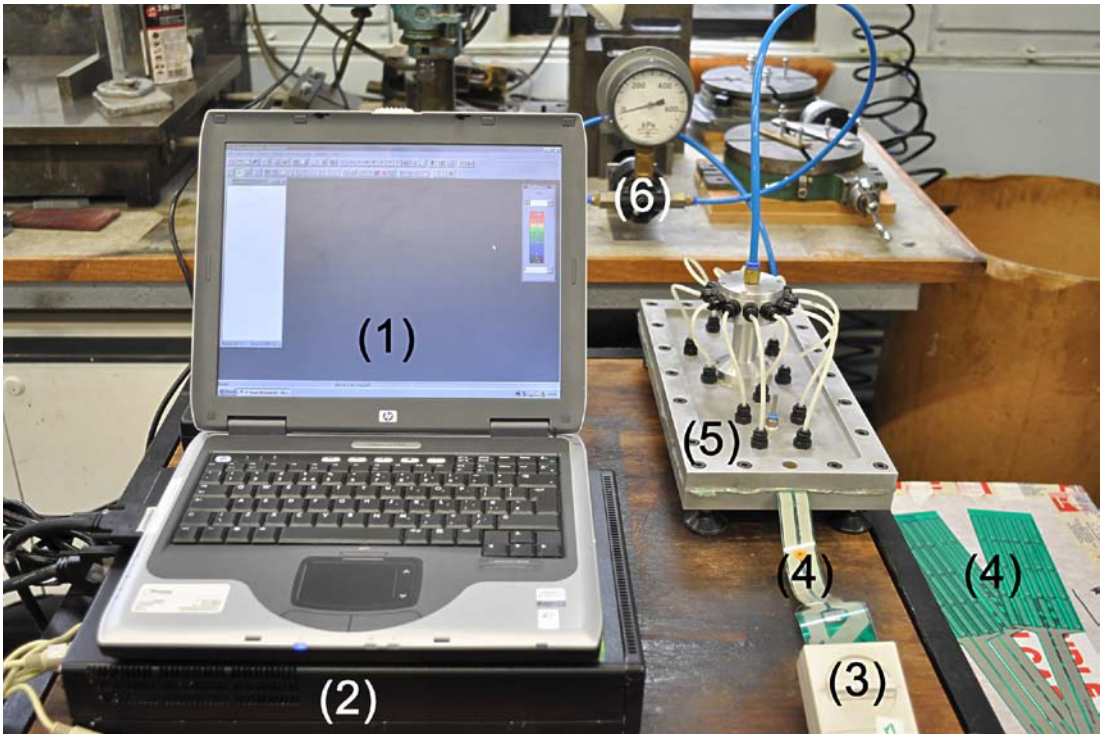

Figure 3-1 The F-Scan system sensor equilibration and calibration set up: (1) laptop computer with F-Scan software, (2) PCI expansion, (3) cuff unit, (4) sensor model 9811, (5) equilibrator, (6) pressure regulator with pressure gauge

After complete equilibration and calibration of all F-Scan system sensors, one model 3000 sensor and three model 9811 sensors were attached in six different places inside the AFO. The model 3000 sensor was positioned beneath the foot by spray adhesive (3M Spray Mount Adhesive, 3M, USA). Three model 9811 sensors were located in central calf, lateral and medial calf, and ankle and strap position by double sided tape (Sellotape, Henkel Ltd, Cheshire, UK) (Figure 3-2).

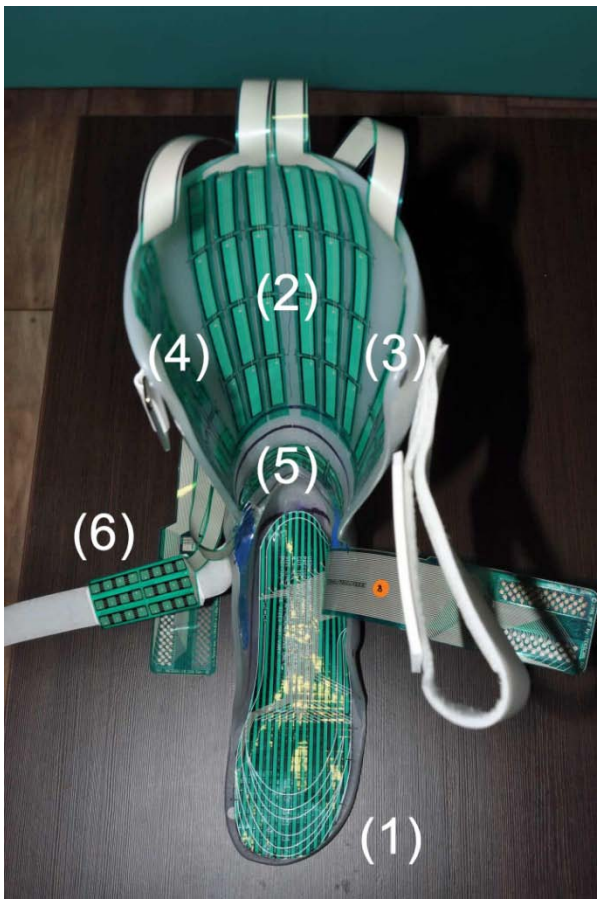

Figure 3-2 Sensor positions: (1) sole, (2) central calf, (3) lateral calf, (4) medial calf, (5) ankle, (6) strap

To perform the F-Scan experiment, the AFO with sensors attached was worn by the subject who has no neurological disorders and no pathological gait. His weight and height are 84.2kg and 168cm respectively. Four sensor tabs extension outside the AFO were then inserted to four cuff units that connected to PCI expansion and laptop computer via four 30ft cuff cables. A Velcro ankle band was applied over the AFO worn by the subject for the cuff units to remain attach to the subject during walking (Figure 3-3). The long cuff cables linked between the cuff units and the PCI expansion allow the subject to walk conveniently and long distance enough to collect the data. Additionally, a wedge was requested by the subject to insert between the AFO and the insole of the shoe at the heel area to change the AFO angle for more convenient walking. Load data was collected as the subject walked with a normal gait for approximately six gait cycles, and this was repeated ten times.

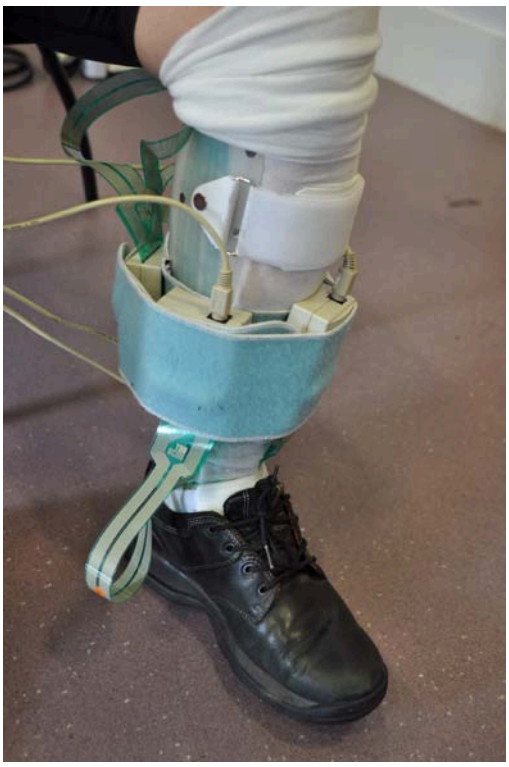

Figure 3-3 The AFO with F-Scan system set up worn by the subject

3.2.2 Data analysis of F-Scan system experiment

The results from the F-Scan system experiment were analysed using the F-Scan Research software (F-Scan Research version 5.83, Tekscan Inc, Massachusetts, USA) together with Microsoft Office Excel 2007 (Microsoft Corp, USA). The data from each test was divided into individual gait cycles based on the plot of the plantar force versus frames (Figure 3-4). The gait cycle could be split into two sections, 60% for stance phase and 40% for swing phase. Stance phase was divided into four components: loading response or foot flat, midstance, terminal stance or heel off, and preswing. As well as swing phase was separated into three components: initial, middle, and terminal swing (Gage, Deluca et al. 1995; Cuccurullo 2004). Four components from both of stance and swing phase, foot flat, midstance, heel off, and midswing, were interested to be pressure analysis points because these points located close to four vertexes of force-frames curve (Figure 3-5). Foot flat, midstance, heel off, and midswing were deemed to be at 10%, 30%, 50%, and 80% of the gait cycle respectively (Whittle 2007).

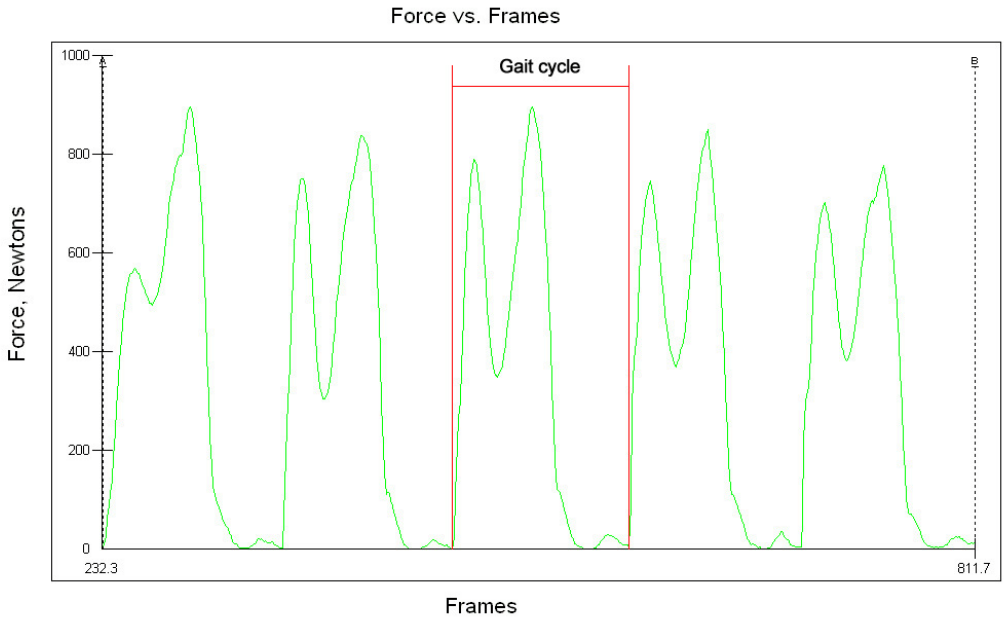

Figure 3-4 A plot of plantar force versus frames

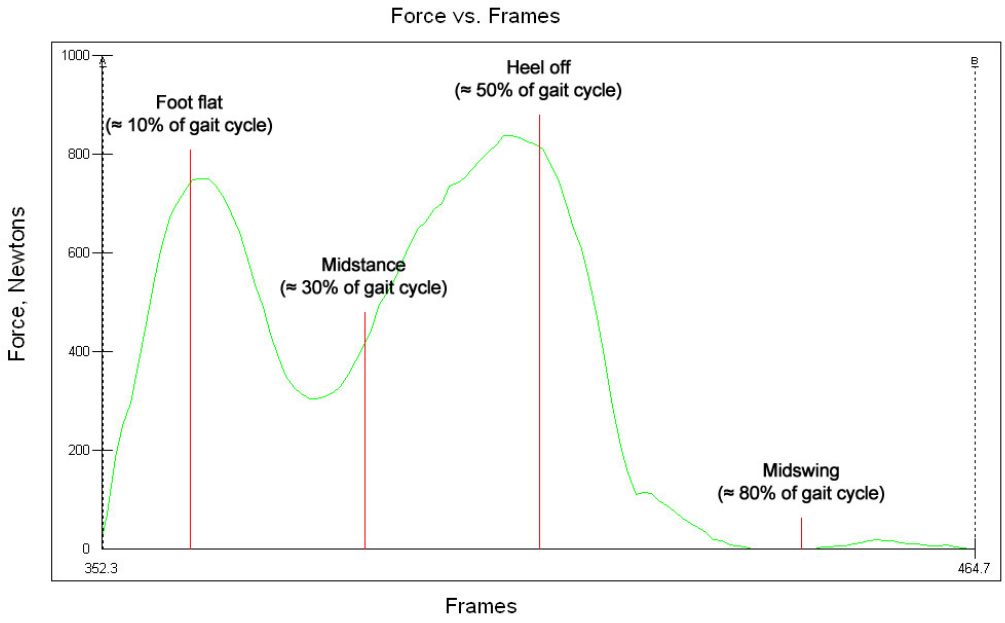

Figure 3-5 Four components in the gait cycle that were analysed

The data acquisition was performed at frequency 100Hz. This frequency is appropriate for adequate capturing the pressure data for analysis. The data from

each test was separated into gait cycles using the position of initial contact or heel strike component. The heel strike position was found by locating the frame where the force started to increase sharply. Seven gait cycles could then be defined, the most complete four gait cycles out of seven were chosen for further analysis.

The data from five positions out of six were split into small sections using F-Scan Research software. The sensor located at the sole area was divided into six sections, and the sensors located at the calf and the ankle areas were split into three equal sections (Figure 3-6). Only the sensor located at the lower strap still was not split up. The contact pressure and the peak contact pressure for all positions could then be quantified from the plot of the pressure versus frame using F-Scan Research software. The pressure data from four gait cycles in each test from ten repeated tests were analysed for each section of each sensor position at each gait component, the average and the standard deviation of contact and peak contact pressure were the results of this analysis.

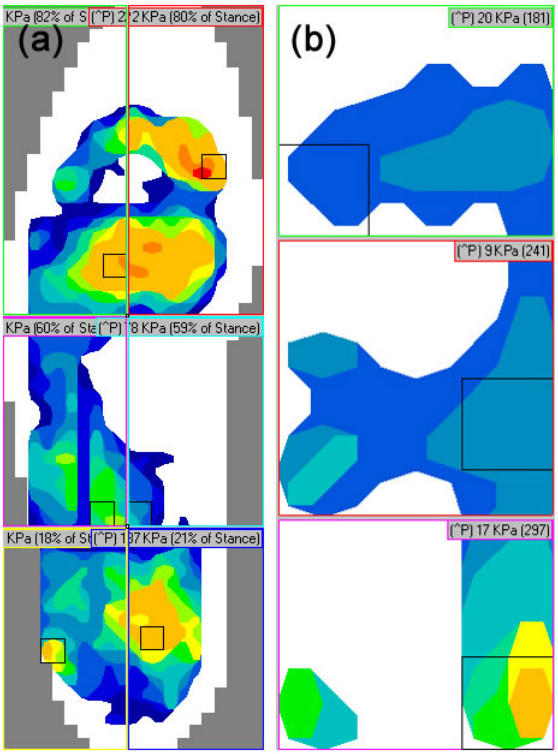

Figure 3-6 (a) plantar sensor split into six sections and (b) central calf sensor split into three sections for analysis using F-Scan Research software

In the beginning of this experiment, a problem about sensor at some positions especially in the calf area could not measure any pressure applied by the subject was found (Figure 3-7). This was thought the problem might be due to lack of area of contact between lower limb of subject and AFO at no pressure measured positions. The shape of AFO was not match with the shape of lower limb of subject making a gap between AFO and limb might be caused of lack of contact area. An ethylene vinyl acetate (EVA) foam sheet 2mm thickness was used to apply on the sensor at the defective position to fill the gap to improve the measurement. The pressure could then be measured at almost of the defective position (Figure 3-8). Consequently, the three-ply EVA foam sheet was applied on the sensor at the central calf position, and the two-ply EVA foam sheet was applied on the sensor at three positions: lateral calf, medial calf, and ankle (Figure 3-9).

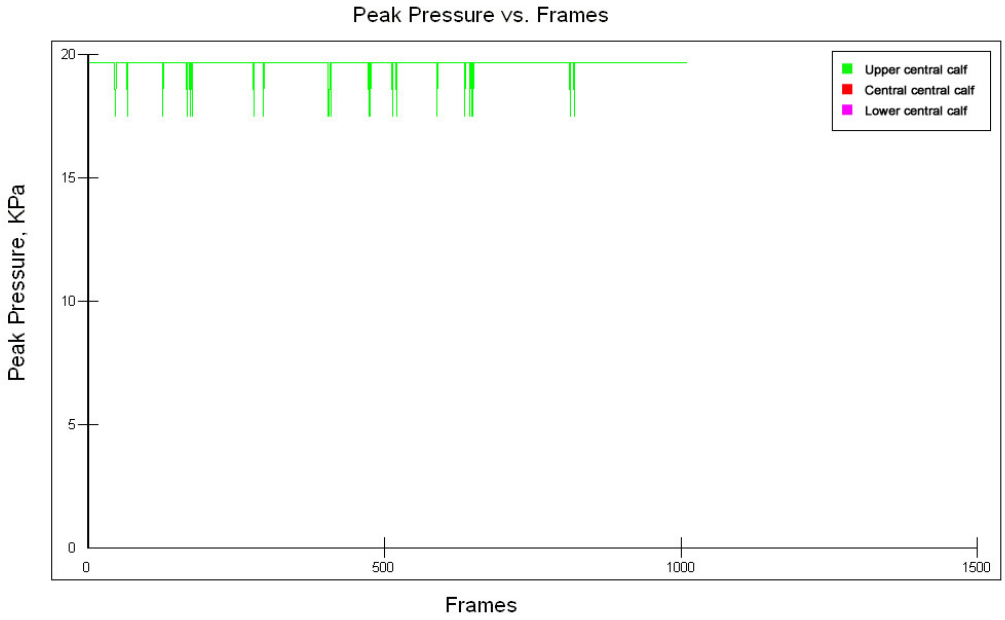

Figure 3-7 Pressure measurement at central calf position without EVA foam sheet applied

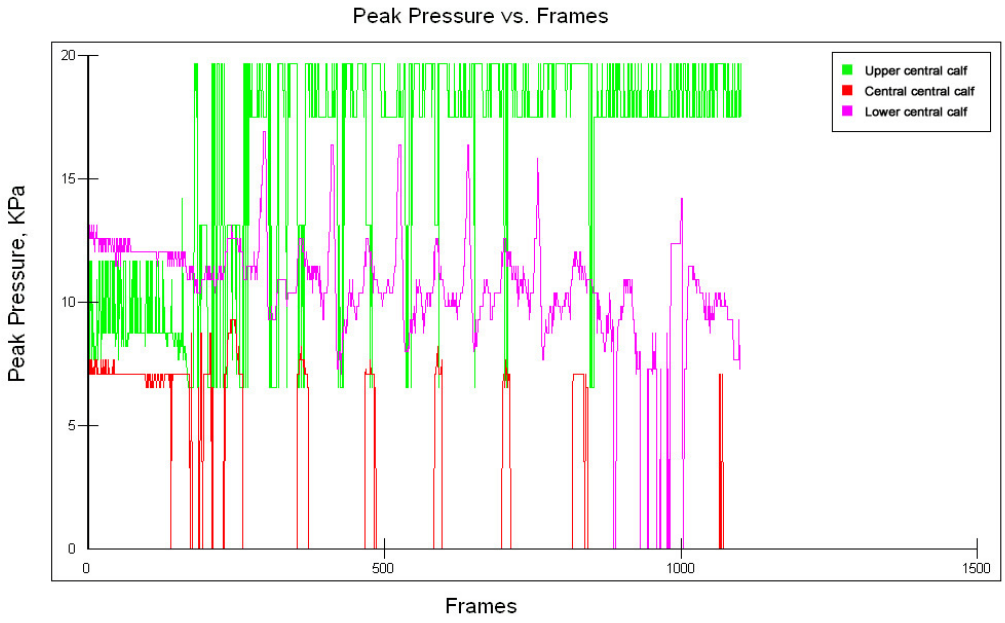

Figure 3-8 Pressure measurement at central calf position with three-ply EVA foam sheet applied

Figure 3-9 EVA foam sheet applying on the sensor at the defective positions

3.2.3 pedar system experiment

According to the novel website, the manufacturer claimed that the pedar system was an accurate and reliable measurement system, and all sensors of the pedar system were individually calibrated using constant air pressure applied to an air bladder with the aid of the trublu® calibration device. The calibration was computer-assisted, and could guarantee accurate and reproducible data. Moreover, the data was transmitted wireless via Bluetooth™ in the pedar system, allowed the subject movement in free range while the user could monitor the change in load and pressure on the screen (Novel 2008).

Due to the pedar system did not need a calibration every use, the sensor calibration was not performed in this experiment. The only one sensor designed specifically for plantar load measurement was positioned beneath the foot on the AFO, hence the pressure in any other areas except the sole were not quantified. The sensor was then wired to the telemetry system to wireless transmit the pressure data collected from the sensor to the laptop computer which pedar software (pedar®-x/E (Expert) software version 12.1.28, Novel GmbH, Germany) already exist to processing via Bluetooth™ (Figure 3-10).

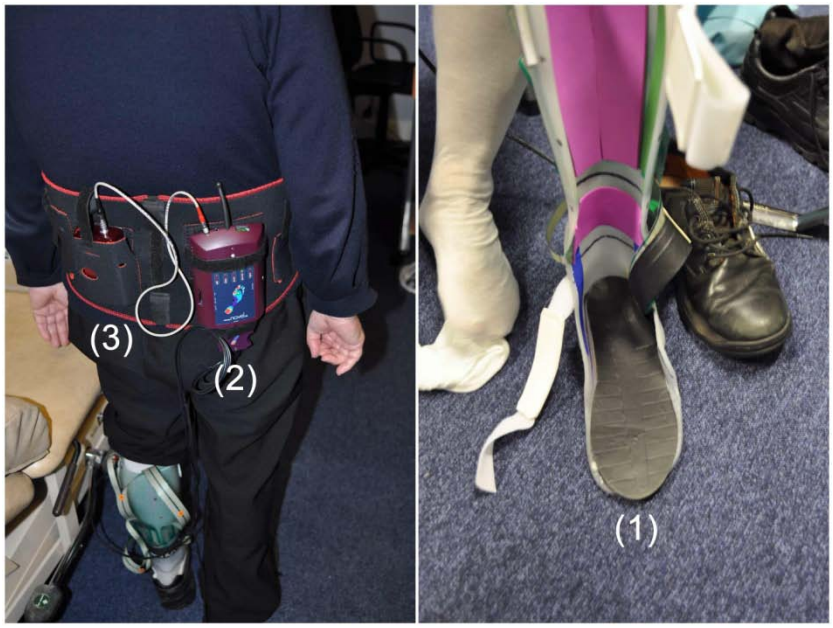

Figure 3-10 pedar®-x system: (1) pedar®-x insole, (2) Bluetooth™ telemetry system, (3) rechargeable NiMH battery

The load data were collected as the subject walked with a normal gait for approximately five gait cycles, and this was repeated eight times.

3.2.4 Data analysis of pedar system experiment

The load data from the pedar system experiment were collected by pedar software (pedar®-x/E (Expert) software version 12.1.28, Novel GmbH, Germany) at a sampling frequency 50Hz (Figure 3-11). After processing, the collected data were then exported as ASCII data to Microsoft Office Excel 2007 (Microsoft Corp, USA) to analysis later. The data from each test was divided into individual gait cycles based on the plot of the plantar force versus time in Microsoft Office Excel 2007 (Figure 3-12).

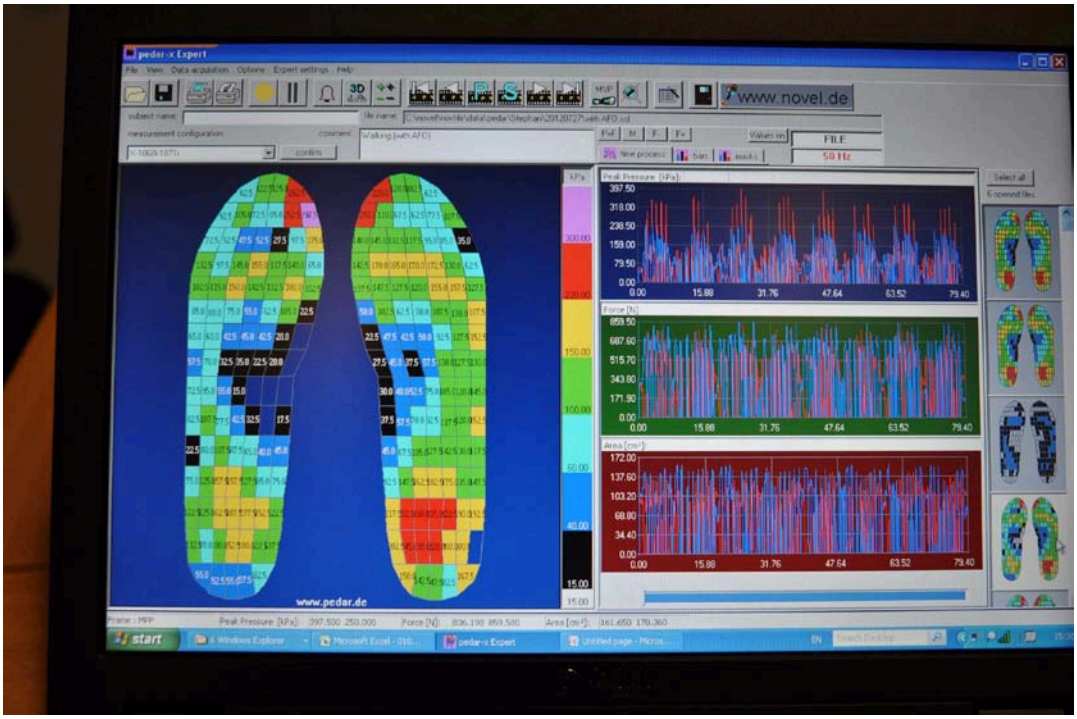

Figure 3-11 pedar®-x Expert software

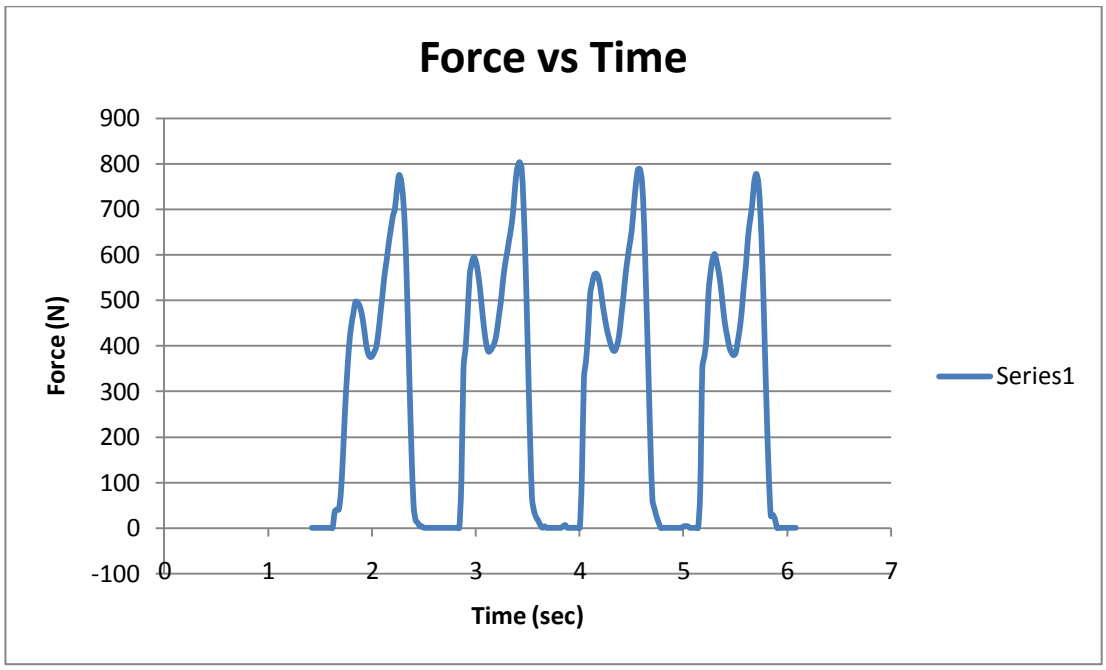

Figure 3-12 Plot of plantar force collected from the pedar system experiment versus time

To comparable with the results from the F-Scan system, the 99 capacitive sensors of the pedar system were divided into groups corresponding to the sections done on the model 3000 sensor in the F-Scan system experiment (Figure 3-13). In the ASCII data, the contact and peak contact pressures could be quantified for each section. The pressure data from four gait cycles in each test were analysed for each section at each gait component, the average and the standard deviation of contact and peak contact pressure were the results of this analysis similar to the results from F-Scan system experiment.

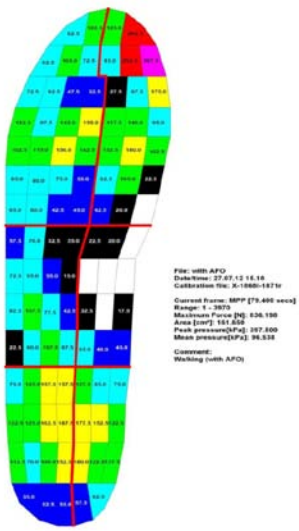

Figure 3-13 Peak contact pressure measured by each sensor throughout the test and sensors divided into sections similar to model 3000 sensor

3.3 Results

3.3.1 F-Scan system experiment

To avoid misunderstanding, the types of the load using in this study must be clarified. Firstly, a force is total force on the sensor area within the region. Secondly, a contact pressure or an average pressure is pressure on the loaded area inside the region calculated by dividing the force by the loaded area. Finally, a peak contact pressure or a maximum pressure is the highest pressure on the loaded area inside the region.

The highest peak contact pressures measured by plantar sensor model 3000 during foot flat and heel off were found at heel and metatarsal area respectively. During midstance, there was no significant difference of the peak contact pressure among three sensor areas: metatarsal, mid foot, and heel. Almost all of sensor areas were not experienced any pressure during midswing (Figure 3-14). In like manner, the contact pressure or average pressure measurement also showed the trend of the results similar to the peak contact pressure measurement (Figure 3-15). A sample of pressure data processed and displayed by F-Scan Research software can be seen in Figure 3-16 showing the peak contact pressure in five gait cycles.

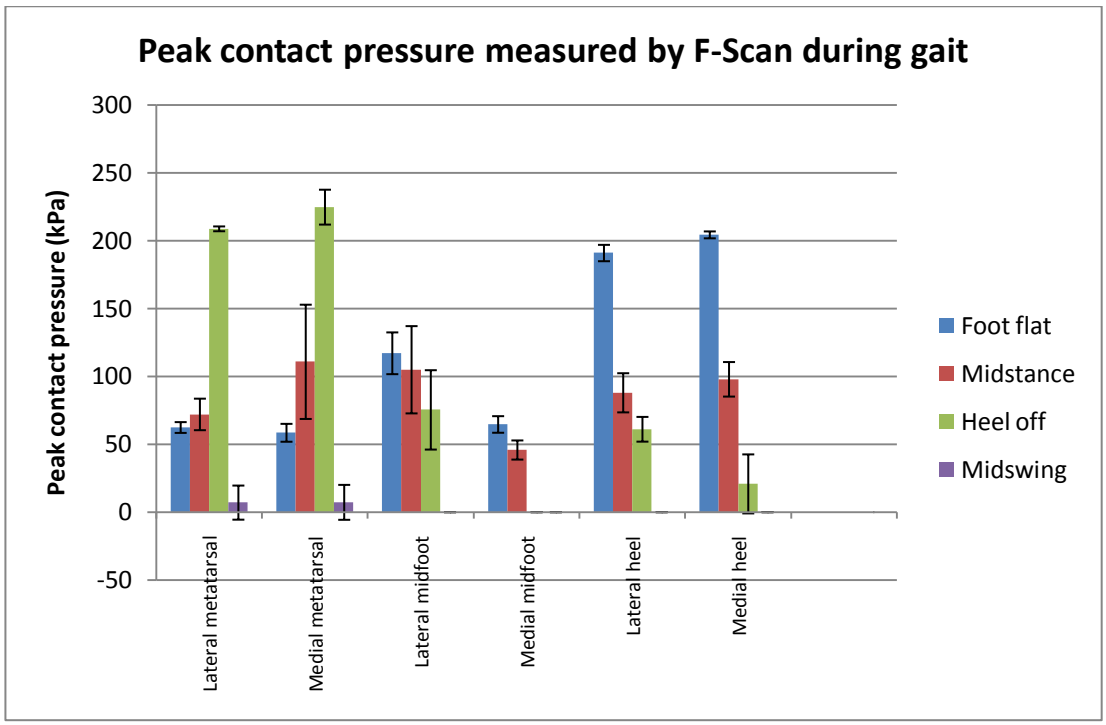

Figure 3-14 Plot of maximum pressure measured by model 3000 sensor during gait

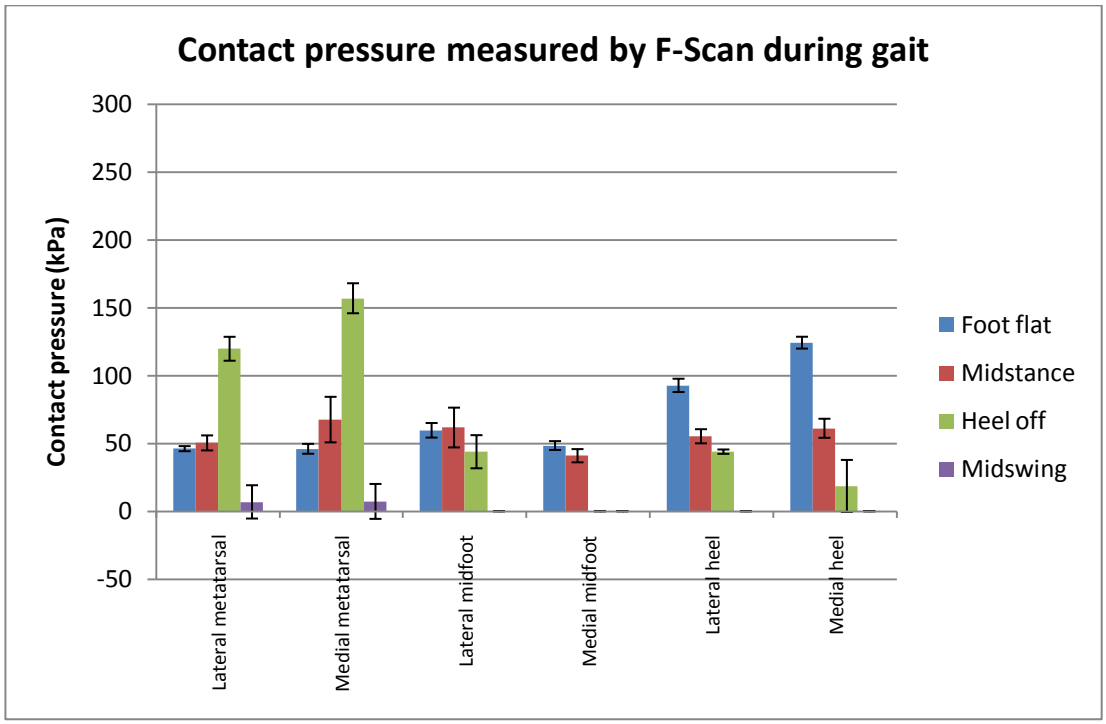

Figure 3-15 Plot of average pressure measured by model 3000 sensor during gait

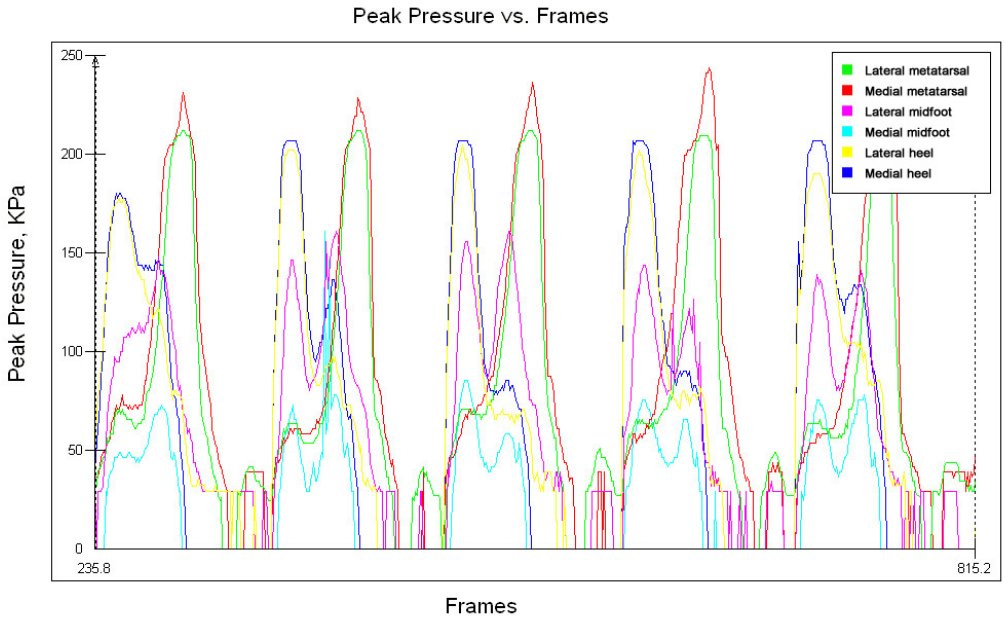

Figure 3-16 Plot of maximum pressure versus frames using F-Scan Research software

The peak contact pressures measured by model 9811 sensors in calf, heel, and strap area during stance phase were considerably lower than the data measuring at the plantar area. The sensor in upper central and central central calf could not be experienced any pressure during almost all of gait components. Some sensors could detect the pressure during swing phase different from the measurement in plantar area that almost all of areas showed no pressure applied (Figure 3-17). The similar trend of the results was shown in the contact pressure measurement as well (Figure 3-18). There was an unknown error occurred in the data displayed in the F-Scan Research software that can be seen in Figure 3-19. The plot always showed the contact pressure measured at 9, 17, and 20kPa, although there was not any detected pressure shown in the sensor map in the same frame.

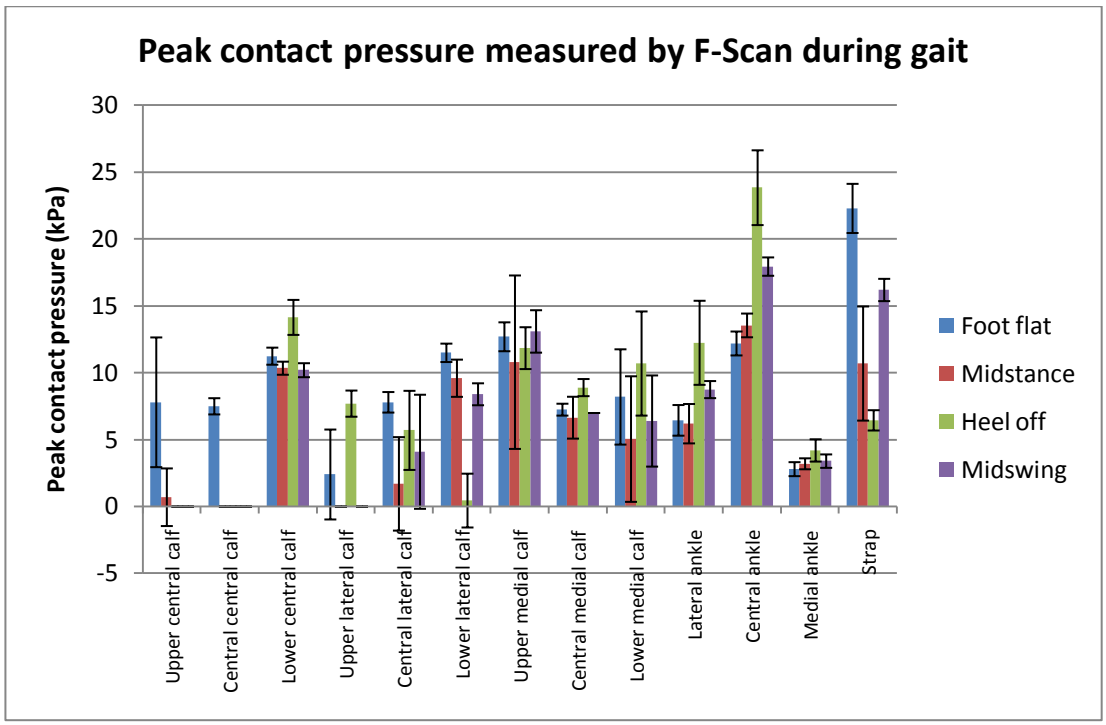

Figure 3-17 Plot of maximum pressure measured by model 9811 sensor during gait

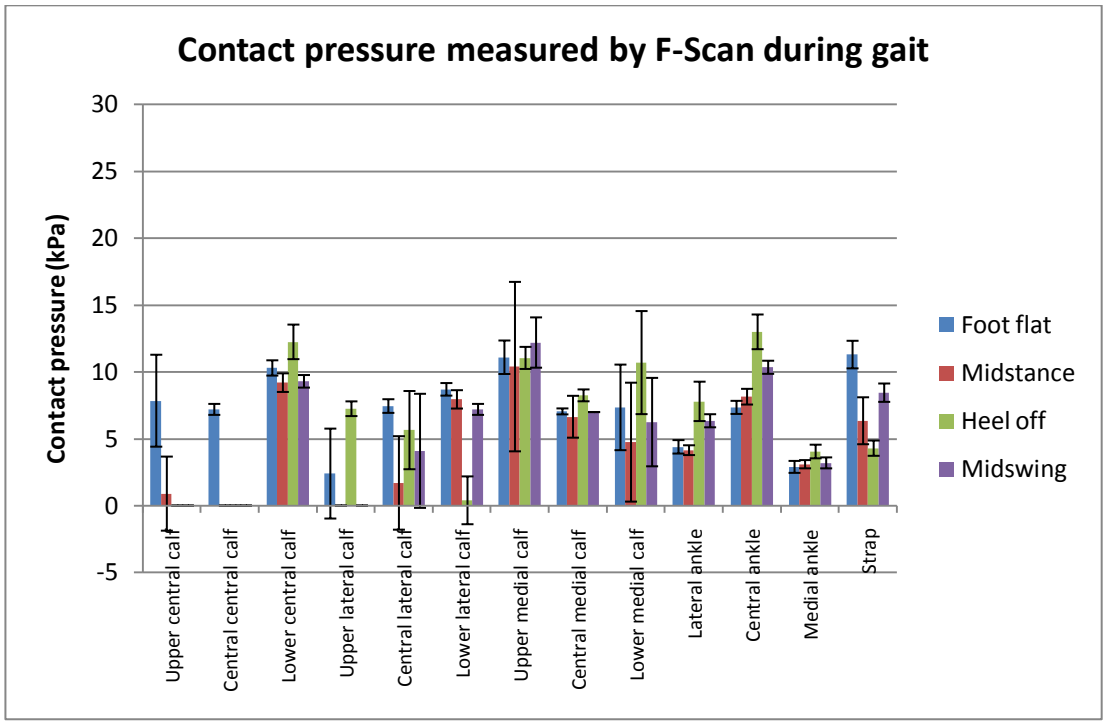

Figure 3-18 Plot of average pressure measured by model 9811 sensor during gait

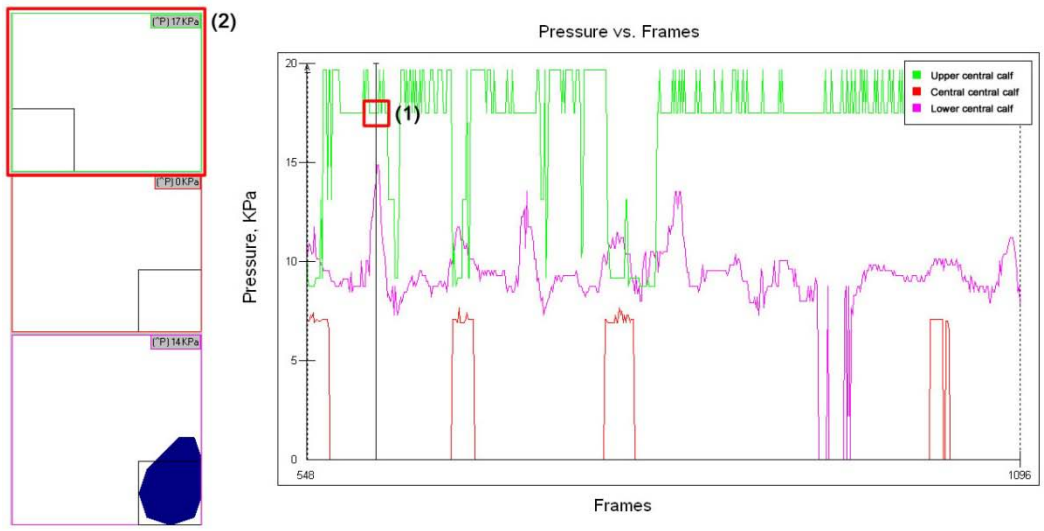

Figure 3-19 The unknown error that the pressure measured shown in the plot (1) does not correspond to the pressure measured shown in the sensor map (2)

3.3.2 pedar system experiment

The highest maximum pressures measured by pedar insole during foot flat and midstance were found at heel area, and during heel off was found at metatarsal area. There was not any measured pressure in all sensor areas during midswing (Figure 3-20). In the same way, the average pressure measurement showed the trend of the results similar to the maximum pressure measurement as well (Figure 3-21)

Due to the pedar insole is designed specifically for plantar load measurement, the pressure measurement in any other areas except the sole were not performed. Consequently, only the plantar pressure was obtained from the pedar system experiment.

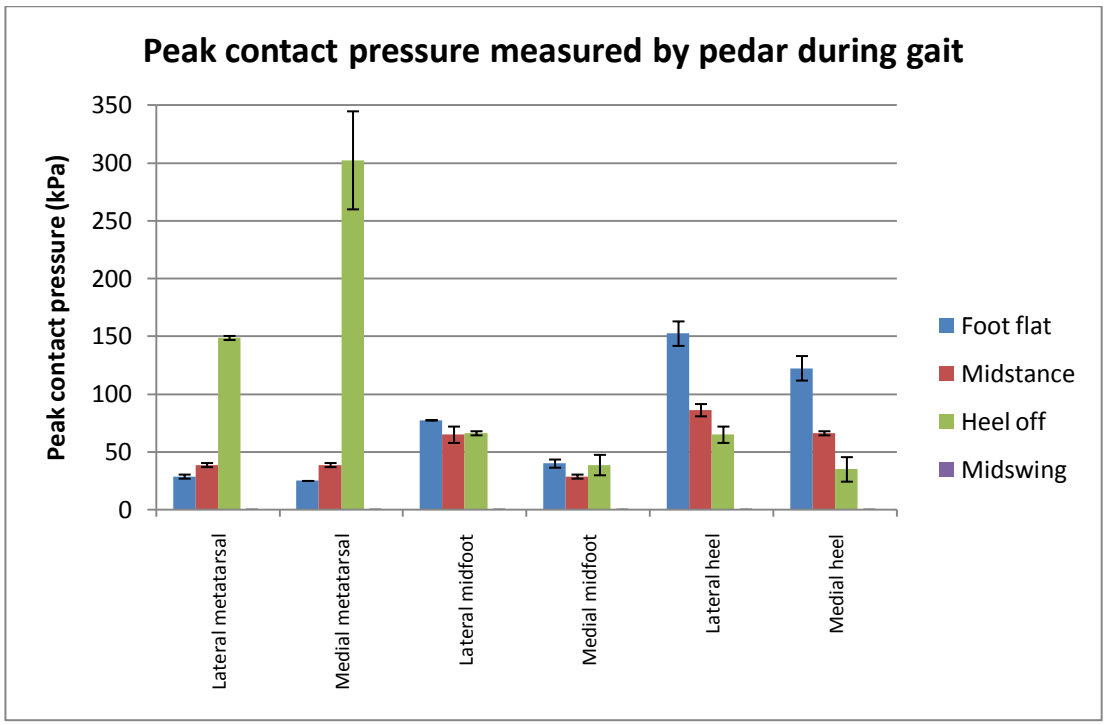

Figure 3-20 Plot of maximum pressure measured by pedar®-x insole during gait

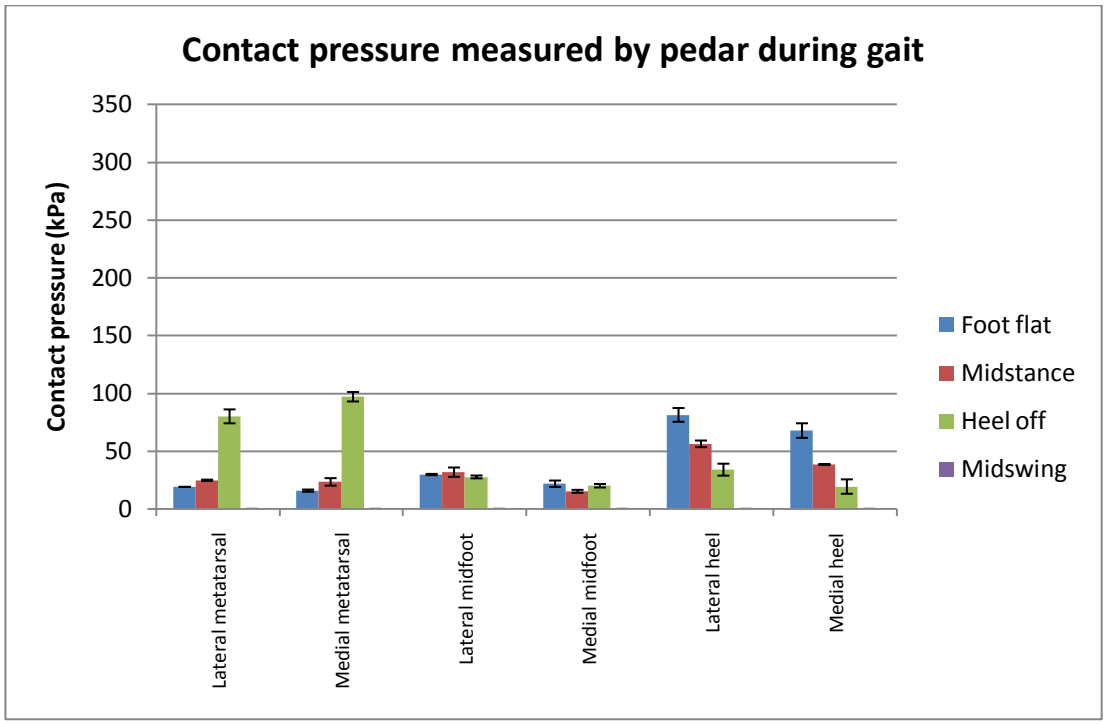

Figure 3-21 Plot of average pressure measured by pedar®-x insole during gait

3.3.3 Comparison between F-Scan and pedar system

The different types of sensor from the different manufacturers were used to measure the similar parameter, the measurement data were then analysed in a way that allow a direct comparison between them. Only the plantar pressure could be compare because the pedar insole could not use to measure load in any others area except the sole due to its specific design.

Due to both of sensor types could not be experienced any pressure in almost all of sensor areas during midswing, the average pressures measured were then be compared during only three gait components: foot flat, midstance, and heel off.

During foot flat, the average pressures measured by both systems showed the similar trend. The highest average pressures measured were located at the heel area, and the lowest average pressures measured were located at the metatarsal area. However, average pressures measured in almost all of sensor areas using the pedar system were only half of the values measured using the F-Scan system (Figure 3-22).

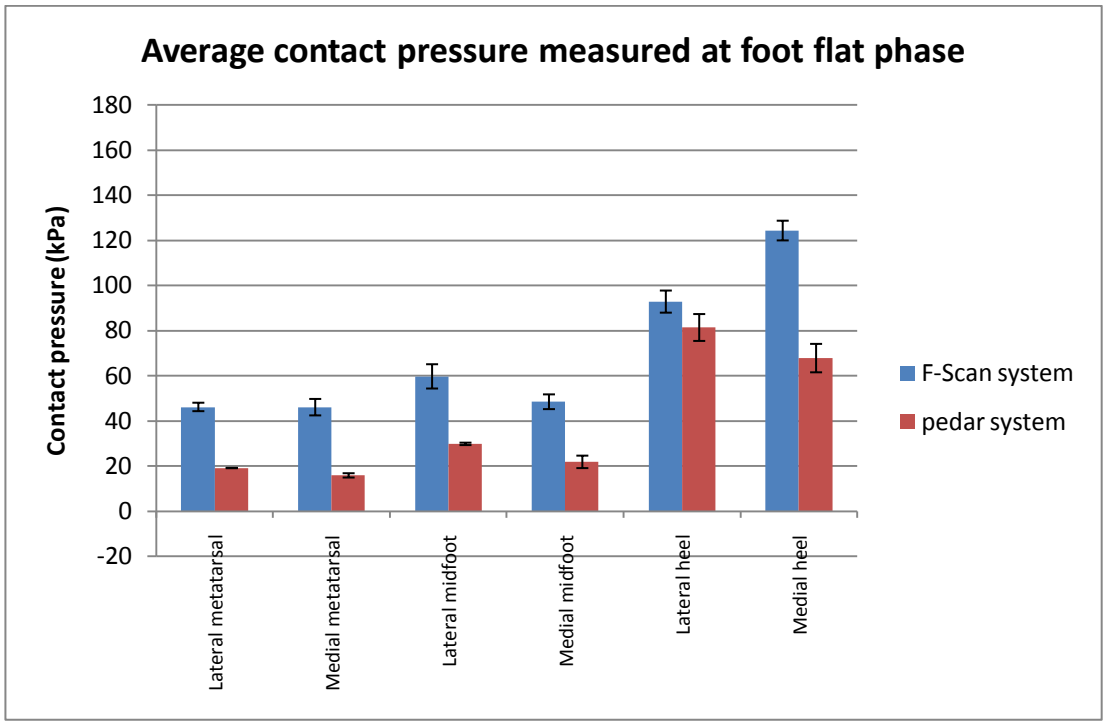

Figure 3-22 Plot of average pressure measured by both systems during foot flat

The average pressures measured by the two systems quite similar during midstance, the measurement values were not much difference among each sensor area. The pressures measured using F-Scan system showed slightly higher at metatarsal area, while the pressures measured using pedar system showed slightly higher at heel area. This might be because a slight difference in percent of gait cycle in the same gait component. However average pressures measured in almost all of sensor areas using the F-Scan system were twice the value of the pressures measured using the pedar system (Figure 3-23).

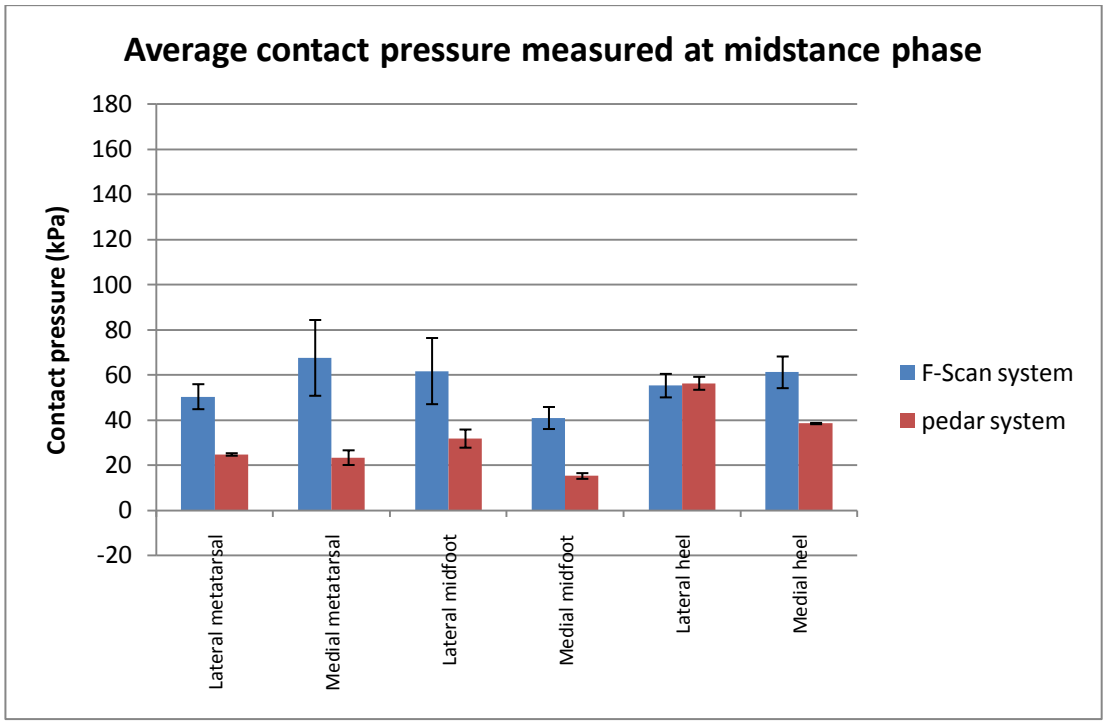

Figure 3-23 Plot of average pressure measured by both systems during midstance

During heel off, the average pressures measured by both systems showed the similar trend. The highest average pressures measured were located at the metatarsal area, and the lowest average pressures measured were located at the heel area. However, the values measured using the F-Scan system were higher than the average pressures measured using the pedar system in almost all of sensor areas (Figure 3-24).

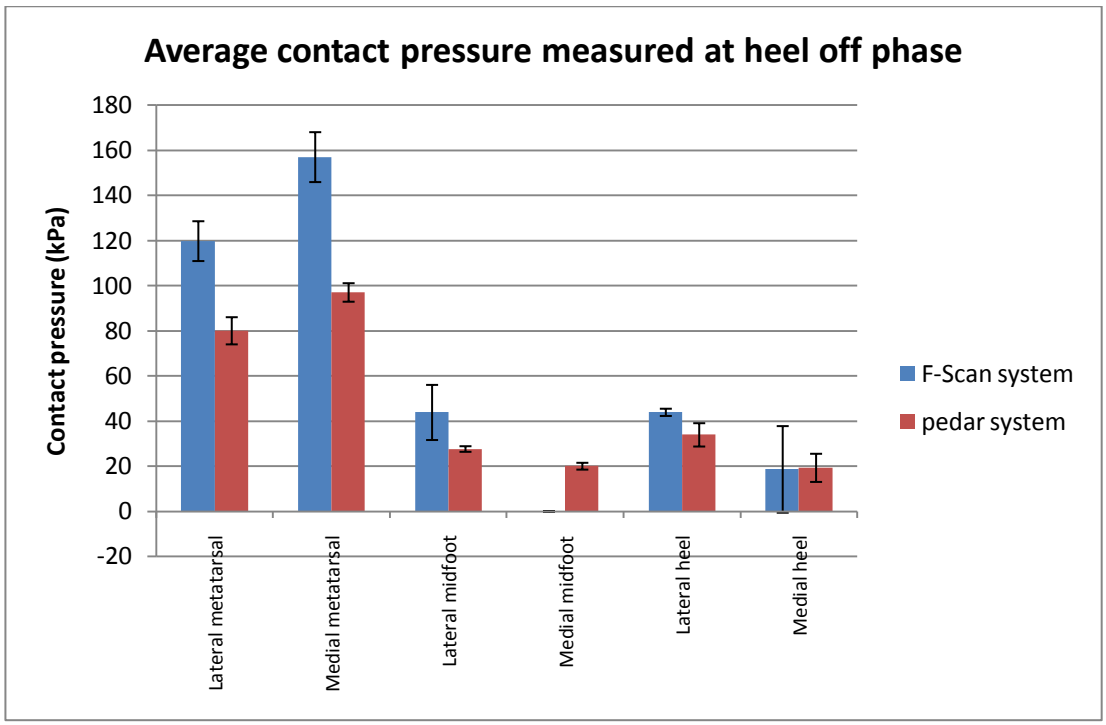

Figure 3-24 Plot of average pressure measured by both systems during heel off

3.4 Discussion

The results gained from the F-Scan system experiment both of peak contact and contact pressure show the measurement values at the plantar area significantly higher than the pressures measuring in other measured areas. In the plantar area, the highest pressure during foot flat is detected at the posterior portion in the heel area, and the highest pressure during heel off is discovered at the anterior portion in the metatarsal area. These findings correspond to the results of the study of Nowak et al. and McHugh (McHugh 1999; Nowak, Abu-Hasaballah et al. 2000). However, the average pressures measured using the F-Scan system in the study of Nowak et al. at lateral and medial metatarsal during heel off are only 24.36% and 21.83% respectively as large as the average pressures measured in this study using the similar measurement system. This might be because a slight difference in percent of gait cycle in the same gait component. The measurement values at the early stance phase cannot compare due to the measurement taken in the different gait component that Nowak et al. measured the pressures at heel strike while the measurement in this study performed at foot flat. During the midstance and midswing, the measurement values in this study are comparable to the results from the study of Nowak et al.

In the other measurement areas except the plantar area using F-Scan system, the measurement values in these areas are quite small compared to the values taken from the measurement in plantar area. Especially in the calf area, some sensors in this study cannot detect any pressures during heel off correspond to the finding in the study of Nowak et al that cannot measure pressure in some area during heel off. This might be because the subjects chosen in both study are non-impaired subjects. The study of McHugh illustrated by the free-body diagrams in the sagittal plane that the magnitude and the direction of forces applied on the calf section of the AFO by the lower limb of the subject depended on the muscle powers. During early stance phase, the magnitude and the direction of forces acted on the calf section of the AFO depended on the power of dorsiflexor muscle group. In the absence of dorsiflexion power, the forces applied on the calf section of the AFO would be occurred while the AFO acted to oppose the plantarflexion moment. On the other hand, the magnitude and the direction of forces applied on the calf section of the AFO during late stance phase depended on the power of plantarflexor muscle group. In the lack of plantarflexion power, the forces acted on the calf section of the AFO would be occurred while the AFO performs to oppose the dorsiflexion moment. Moreover, the magnitude and the direction of forces applied on the lower strap of the AFO by the lower limb of the subject depended on the muscle powers as well. During swing phase, in the absence of dorsiflexion power, the magnitude of the forces applied on the lower strap of the AFO would be higher than other phases while the strap acted to oppose the plantarflexion moment. The measurement values of the force applied on the calf section and the lower strap of the AFO would be low when the normal subjects who had sufficient both of dorsiflexor and plantarflexor muscle group were chosen to perform the test. As can be seen, the overall trend of the results from F-Scan system experiment both of the high pressures measured at the plantar area and the low pressures measured at the calf and lower strap area correspond to the literatures (McHugh 1999; Nowak, Abu-Hasaballah et al. 2000).

The unknown error about the graphical display in the F-Scan Research software is always occurred during analysis and display the result of the measurement in the small load applied areas. In this case, the graph always shows some constant values as the results of the measurement while the sensor map does not detect any measurement values in the same frame (Figure 3-19). The state of the plot is always reaching a plateau at the same constant value should be suspected of error.

Actually, the sensor map and the graph should display the corresponding measurement values because the plot contains the trace that represents the data in the sensor map (Tekscan 2006). To prevent any mistake, the process to obtain the numerical data from F-Scan Research software should be performed carefully. Both of the sensor map and the plot should be always considered together when collecting data. The error might be caused by either hardware or software. The study of Woodburn et al. reported the hardware defects of the F-Scan system such as lack of durability, significant error in calibration, poor creep property, poor hysteresis property, and poor overall repeatability (Woodburn and Helliwell 1996). There is rarely hardware problem found in this study due to the sensors used are brand new sensors and were repeated approximately 60 cycles that much less than 1000 cycles repeatability test in the study of Woodburn et al. However, an important step that should not be neglected is the sensor installation. Due to the F-Scan system working based on the principle of the electrical resistance that is inversely proportional to the distance between the two surfaces of sensing elements, the sensor should be installed with care especially in small radius curve surface that can affect the gap in sensing elements making the measurement results inaccurate. To prevent any error caused by hardware, the calibration or any operation should be performed carefully and strictly follow the user manual.

The results obtained from the pedar experiment are only the pressure measured in plantar area because the pedar insole is designed specifically for plantar load measurement. Both of maximum and average pressure measured using pedar system illustrates the highest pressure during foot flat found at the posterior portion in the heel area, and the highest pressure during heel off detected at the anterior portion in the metatarsal area similar to the trend of results gained from F-Scan system. These findings also correspond to the average pressures measured in the experiment of Nowak et al. (Nowak, Abu-Hasaballah et al. 2000), and the values from three gait components: midstance, heel off, and midswing can be compared to provide the difference in magnitude of the average pressures measured. During heel off, the average pressures measured using the F-Scan system in the study of Nowak et al. at lateral and medial metatarsal are only 36.45% and 35.32% respectively as large as the average pressures measured in this study using the pedar system. There is no pressure measured by all sensors in plantar area during midswing in both studies. The values measured during midstance using the pedar system only in the midfoot and heel area are comparable to the results from the

study of Nowak et al., while the pressure measures in lateral and medial metatarsal in this study are 38.73% and 27.89% respectively as large as the values in the literature (Nowak, Abu-Hasaballah et al. 2000). This might be because a slight difference in percent of gait cycle in the same gait component. Although there are differences in the magnitude of some measurement values, the overall trend of the results using pedar system still corresponds to the study of Nowak et al.

The results from the two different types of sensor from the two different manufacturers in this study illustrate that the overall trend of the two sensors is obviously similar during the three gait components except the midstance phase, and also corresponds to the findings from the literatures (McHugh 1999; Nowak, Abu-Hasaballah et al. 2000). During the midstance, the overall trend of the two sensors is slightly difference (Figure 3-23). The highest pressure measured using the F-Scan system found at the sensor in the metatarsal area, unlike the highest pressure measured using the pedar system detected at the sensor in heel area. This is thought to be a possible result instead of an error. In fact, the results during foot flat, heel off, and midswing show the obviously similar overall trend, and the two experiments using the two different systems are performed separately. A likely reason affects the difference in overall trend during midstance phase should be a slight difference in percent of gait cycle in the same gait component. Refer to the gait cycle (Gage, Deluca et al. 1995), the pressure values gained from the F-Scan system might be captured in a split second or a few percent of gait cycle pass the midstance phase due to the highest pressure located in the metatarsal area, while the pressure values obtained from the pedar system might be taken in a split second or a few percent of gait cycle before the midstance phase because of the highest pressure located in the heel area.

With attention to the difference in the magnitude of the pressures collected from the two sensors in the same measurement area, the several reasons can be the cause of this problem such as the calibration, the sensitivity, the accuracy, and the repeatability. The study of Woodburn et al. claimed that the F-Scan system was lack of durability, significant error in calibration, poor creep property, poor hysteresis property, and poor overall repeatability (Woodburn and Helliwell 1996). Moreover the study of Quesada et al. reported that the pedar system had a greatest accuracy and a greatest repeatability (Quesada, Rash et al. 1997). To sum up, the authors recommended to avoid using the F-Scan system, and encouraged to use the pedar

system. Nevertheless, the study of Quesada et al. also suggested that the F-Scan system could be improved by using the brand new sensor and calibrating via bladder.

Consequently, the pressure data gained from the F-Scan is chosen to use for further analysis in the finite element analysis software because of three reasons: the F-scan sensors using in this study are brand new, the F-Scan sensors are calibrated via bladder, and prefer to use the similar type of sensor in all measurement areas.

Chapter 4 3D scanning

4.1 Introduction to 3D scanning

Three-dimensional (3D) scanning is usually performed by a device called a 3D digitiser, which records x, y, and z coordinates of a real object to collect data on its shape. The collected data, a point cloud, can then be used to extrapolate the shape to construct a 3D graphics of the subject. A variety of technologies used to digitally acquiring the geometry of a 3D object, one is a contact 3D digitiser that investigate the subject through physical touch, and another one is a non-contact 3D digitiser that investigate the shape by detect the reflection of light on the subject surface. A digital 3D model acquired from the 3D scanning can be useful for a wide variety of applications such as computer-aided design (CAD), computer-aided manufacturing (CAM), and finite element analysis (FEA).

In like manner, a digital 3D model of the AFO used in this study needed to be done by the 3D scanning that was considered to be one of the most rapid and accurate methods.

4.2 Methodology and instrumentation

The AFO used in this study was made individually for the subject without pathological gait by the National Centre for Prosthetics and Orthotics (NCPO), University of Strathclyde, Glasgow, UK. The AFO used in this study was custom-molded, solid-ankle AFO made of homopolymer polypropylene (North Sea Plastics Ltd, Glasgow, UK) by thermoforming process with carbon fiber reinforcement (Fillauer Companies Inc, Tennessee, USA) at the malleolus position (Figure 4-1).

Figure 4-1 Homopolymer polypropylene AFO made by NCPO

The non-contact 3D digitiser (VIVID 9i/VI-9i, Konica Minolta Optics Inc, Japan) was used to investigate the geometry of the AFO. The scanning could not perform directly on the AFO surface due to the homopolymer polypropylene that the AFO made of is a translucent material. The amount of reflection detected by the 3D digitiser was inadequate to construct the good quality 3D digital model. This might be because either the subsurface scattering in a translucent object can shift the observed intensity peak away from the point of incidence, or opaque structures beneath the surface pollute the range estimate (Tongbo, Lensch et al. 2007). A suspension of an inert white powder in a quick drying solvent (Ardrox 9D1B, Chemetall GmbH, Germany) was sprayed on the AFO surface to improve reflection (Figure 4-2). Before the scanning was started, the 3D digitiser had been performed the field calibration correspond to the type of lens, the middle lens, used follow the instruction manual.

Figure 4-2 (a) powder sprayed on AFO surface and (b) Ardrox 9D1B

The surface prepared AFO was set up at about one meter in front of the calibrated 3D digitiser for the scanning (Figure 4-3). The AFO was taken 12 scans at 20° intervals on calf and foot area, and four scans at 20° intervals on sole area. The scanning data was transferred from the 3D digitiser to the computer via USB cable, and initially processed by Polygon Editing Tool software version 2.40 (Konica Minolta Sensing Inc, Japan) then saved as an element file type preparing for the next process.

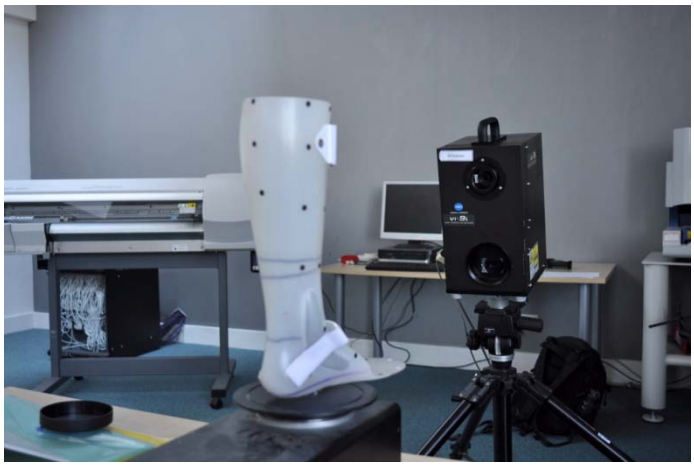

Figure 4-3 AFO and 3D digitiser set up for scanning

The 16 element files were imported into Geomagic Studio software version 10 (Geomagic studio 10, Geomagic Inc, USA). In this software, an object always existed in one of several phases:

- Point phase: the state that the object was a collection of scanned points.
- Polygon phase: the state that the appearance of the object was approximated by drawing a triangular surface between every three data points.
- Surface phase: the state that a reproducible surface was being applied over underlying polygon mesh of the object.
- CAD phase: the state that the object was ready for perform trimming or Boolean operations (Geomagic 2008).

Before the point phase, the 16 elements were aligned together using the manual registration command that could achieve two elements each time. The common three points located on each element was used to define the correct position in assembly. This command was repeated until complete the alignment of all 16 elements. Then all elements in the correct position were transformed to groups of point cloud in the point phase. The excess scanned data was deleted manually, the extraneous data points were reduces using the reduce noise command, and all groups were merged together using merge point objects command. The final step in the point phase was the polygon object created using the wrap command. In the polygon phase, the polygon object was prepared for moving to the surface phase such as filling the gaps in the polygon surface. The object with good patch structure with regular shaped patches that fill spaces efficiently was created during surface phase. Subsequently, the NURBS surface was generated, the object could then be moved to CAD phase to save CAD object as an IGES file for further processing by other software.

Moreover, NX 7 software (Siemens Product Lifecycle Management Software Inc, Texas, USA) was chosen for the next step of CAD data processing. The IGES file was imported to this software, and the 3D model of the AFO was then moved to the appropriate position on a 3D Cartesian coordinate system. The model was implemented by the various commands in this software such as drilling the holes for the strap rivets. The final step in NX 7 software is the modified 3D model was saved as a Parasolid file for analysis by ANSYS 14.0 software (ANSYS Inc, Pennsylvania, USA).

4.3 Results

The 16 scanned data acquired from Polygon Editing Tool software was adequate to construct the 3D model of the AFO finely (Figure 4-4). The more data the AFO was scanned, the more accuracy the 3D model was constructed. This was because there was an overlap area on each scan that could be used to confirm one another the correct shape of the subject. After the scanned data had been collected from the 3D digitiser, the data was saved as the element file in this software and exported to Geomagic software for further processing.

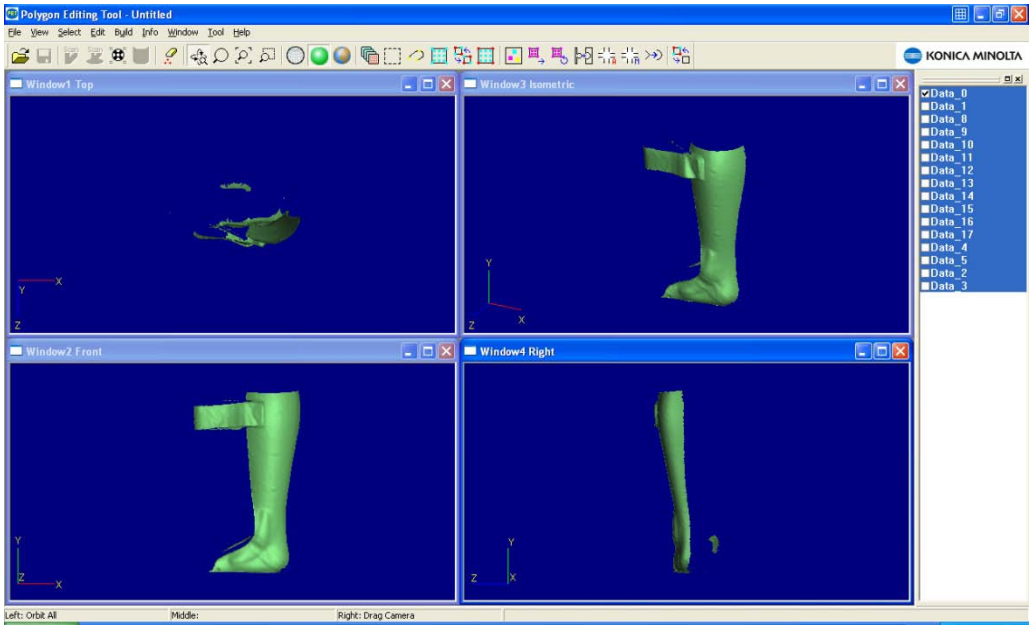

Figure 4-4 Scanned data collected from 3D digitiser in Polygon Editing Tool software

There were five steps performed in Geomagic software to improve quality of the scanned data. The results of each step taken in this software are illustrated in Figure 4-5. Image (a) and (b) shows the 16 imported element data before and after alignment respectively. A transformation from 16 elements to 16 point cloud groups is shown in image (c). In this step, an excessive data and a noise were eliminated manually and automatically, the point cloud groups were then merged together. The third step is shown in image (d), the triangular surface was drawn among every three points to create polygon. Either hole or gap was also implemented in this step. Image (e) illustrates the surface model the result of surface constructed based on

the polygon mesh. The final step, the surface model was transformed to CAD model ready to save as IGES file and export to the CAD or analysis software later, the result is shown in image (f).

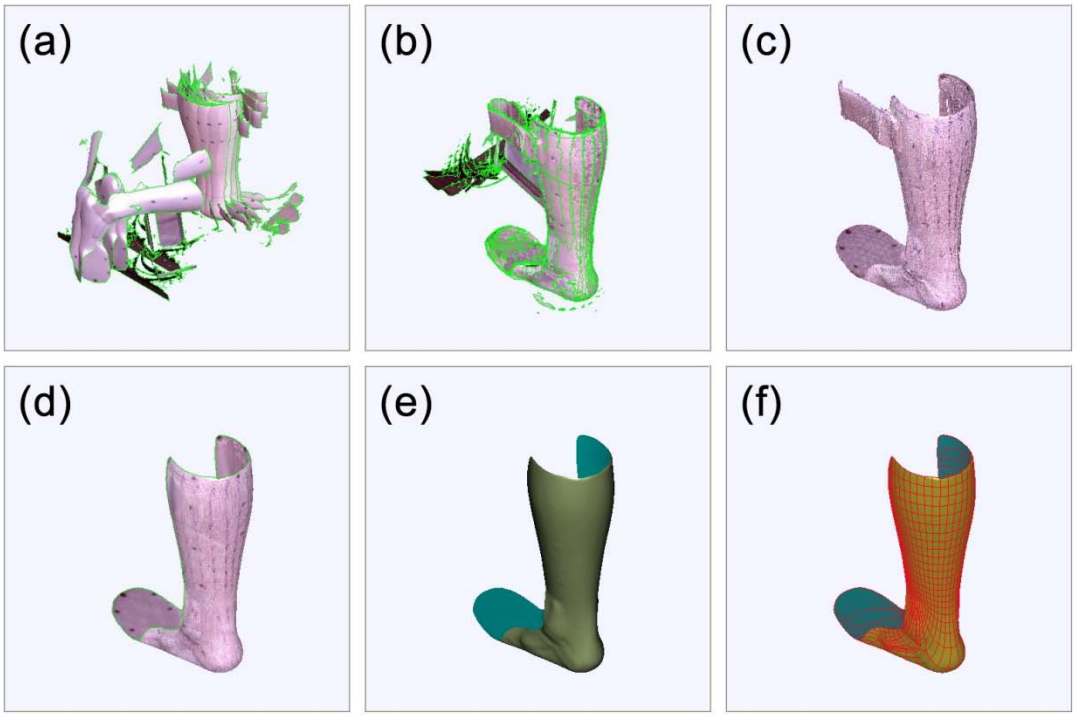

Figure 4-5 Five steps of scanned data improvement in Geomagic software

Figure 4-6 shows the result from NX software, the IGES model acquired from Geomagic software was changed to the appropriate position based on 3D Cartesian coordinate system. The 3D model was also decorated similar to the real objected condition, such as drilling three holes 4mm in diameter on the model for the three strap rivets. Then, the modified model was saved as a Parasolid file for finite element analysis in ANSYS software further.

Figure 4-6 Complete Parasolid file acquired from NX software

4.4 Discussion

Due to the homopolymer polypropylene sheet used to make the AFO is a translucent material, the 3D scanning done by the non-contact 3D digitiser that working based on the reflection cannot perform well enough on this surface type, the powder spray is needed to use to prepare the AFO surface before scan. Either the subsurface scattering in a translucent object can shift the observed intensity peak away from the point of incidence, or opaque structures beneath the surface pollute the range estimate might be the cause of the trouble in scanning (Tongbo, Lensch et al. 2007). The surface of the scanned data gained from scanning on AFO surface without powder sprayed is rough and cannot be accepted for using (Figure 4-7), spraying powder on the AFO surface can improve the quality of the scanned data. Although the powder was sprayed on the AFO surface to make it more opaque, the different thickness of the sprayed powder on the AFO surface might cause the difference in reflection that affect to the detection system of the 3D digitiser make the scanned data inaccuracy. This is one of the several factors making some error in 3D scanning.

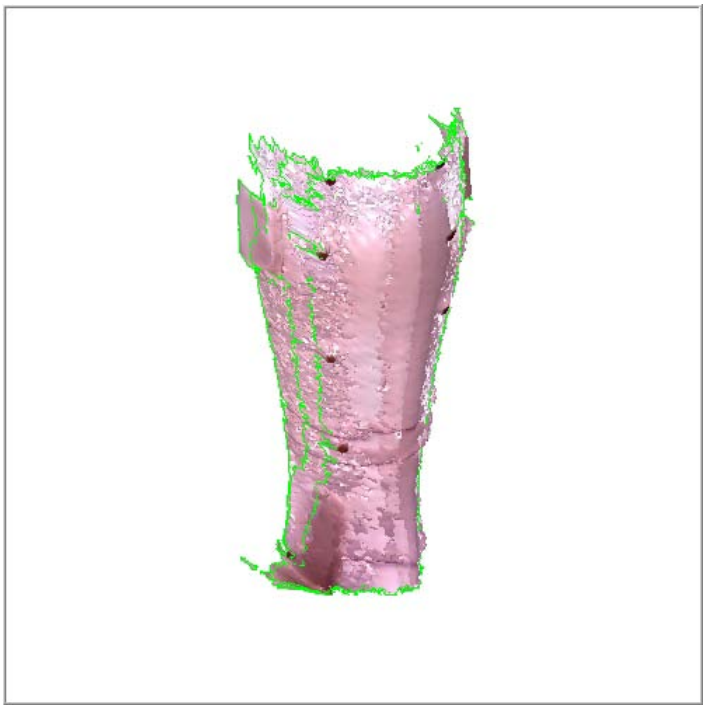

Figure 4-7 Rough scanned data scanning on AFO surface without powder sprayed

Another possible factor of error in the 3D scanning might occurred during the calculation process in the software. Due to the polygon model was constructed from the point cloud by drawing the triangular surface among every three points, some scattered points such as noise and outlier that cannot be completely eliminated affect the drawing make the triangular surface incorrect both of shape and position. The continued process constructing the object surface based on these triangular surfaces was affected as well. Consequently, the final result of surface construction is inaccuracy and difference from the real object due to the accumulate error in the prior processes.

Some error might be occurred during both of object scanning and data calculating process, however, the 3D scanning was considered to be the most rapid and accurate method to capture the geometry of the real object to create its digitally 3D model. To reduce the error, the scanning and the data processing should be performed carefully and strictly follow the instruction manual.

Chapter 5 Finite element analysis

5.1 Introduction to finite element analysis

The finite element analysis (FEA) is a practical application of the finite element method (FEM). The FEM is a numerical technique used to obtain approximate solutions of boundary value problem, a mathematical problem in which one or more dependent variables must satisfy a differential equation everywhere within a known domain of independent variables and satisfy specific conditions on the boundary of the domain, in engineering (Hutton 2004). The first development of the FEM can be found in the work by Alexander Hrennikoff, a Russian engineer, in 1941 and Richard Courant, a German mathematician, in 1942. At the present time, the FEM is widely used in product design and development that allows a design to be constructed, refined, and optimised before manufacturing.

ANSYS (ANSYS Inc, Pennsylvania, USA) is a general-purpose FEA software for numerically solving a wide variety of mechanical problems including static or dynamic, linear or nonlinear structural analysis, heat transfer, fluid, acoustic, and electromagnetic problems. By and large, the FEA solution might be divided into three stages identified as follows:

- Preprocessing: defining the problem
- Solution: assigning loads, constraints, and solving
- Postprocessing: further processing and viewing of the results (Nakasone, Yoshimoto et al. 2006).

To predict the stresses and strains acting on the AFO, the results from the two previous chapters, the pressures applied on the AFO and the 3D scanned model of the AFO, were simulated together using FEM in ANSYS software.

5.2 Methodology and instrumentation

This section explains the methods to prepare the FE model to analyse using ANSYS software to gain an accurate result.

5.2.1 Geometry

Material properties and geometric properties are defined in this section.

5.2.1.1 Material properties

The AFO used in this study was custom-molded, solid-ankle AFO was made of homopolymer polypropylene (North Sea Plastics Ltd, Glasgow, UK) by thermoforming process. To analyse using software, the material properties: density, Young's modulus, and Poisson's ratio were required.

The density of homopolymer polypropylene using in this study was 909.0909kg/m^3 quantified by dividing mass of a homopolymer polypropylene specimen by its volume. 0.049kg and 0.0000539m^3 were mass and volume of the specimen.

The Young's modulus using in this study quantified from data of a 200-cycle homopolymer polypropylene tensile test done by Enrica Papi, a PhD student in Department of Bioengineering, University of Strathclyde, in April 2009 (Figure 5-1). This value was 2050.1MPA obtained from the slope of the stress-strain curve of one cycle in the tensile test (Figure 5-2).

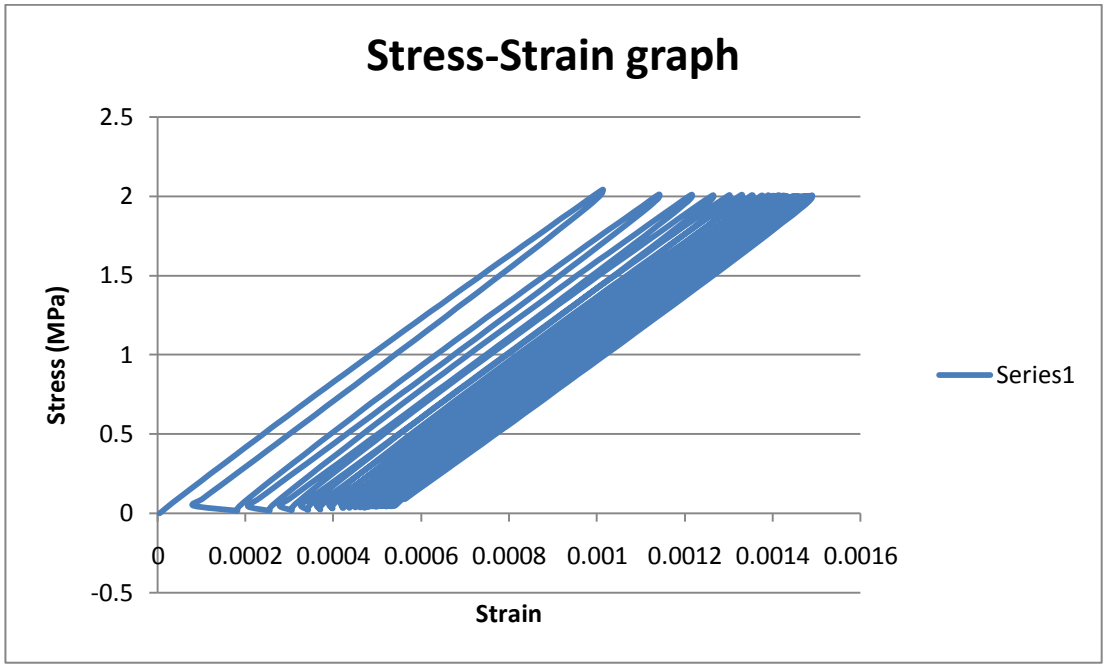

Figure 5-1 Plot of stress-strain data gained from homopolymer polypropylene 200-cycle tensile test done by Enrica Papi

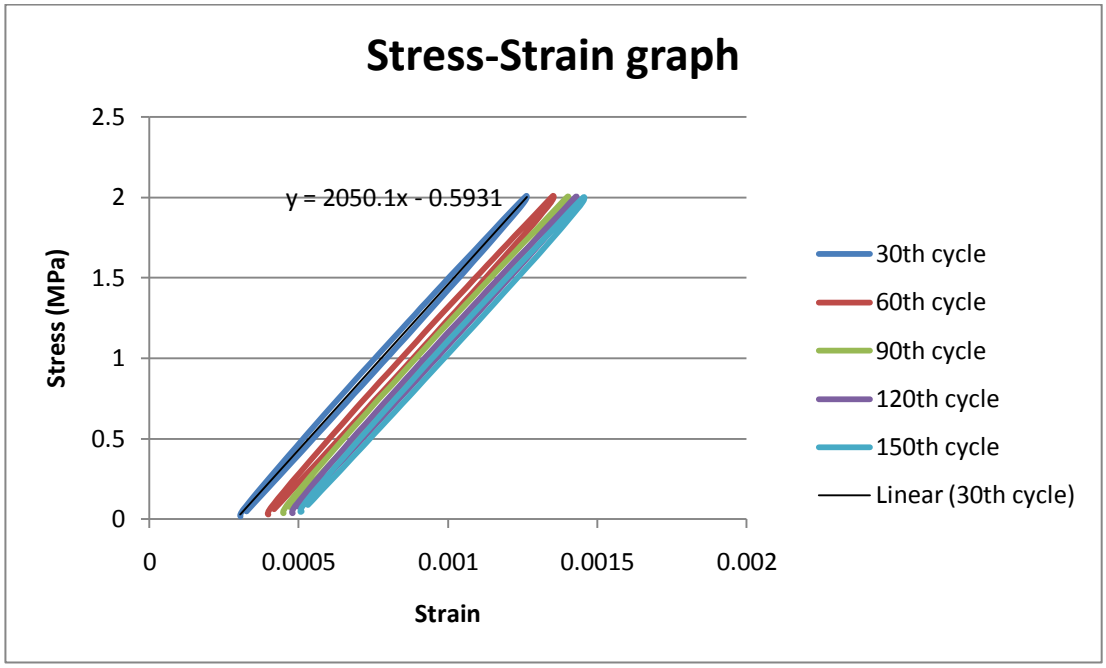

Figure 5-2 Young's modulus quantified from the gradient of the 30th cycle stress-strain curve

The Poisson's ratio of the homopolymer polypropylene obtained from website of a polypropylene manufacturer in USA, INEOS Olefins & Polymers USA, is 0.45 (INEOS 2010).

5.2.1.2 Thickness

The thickness of AFO was measured at 33 different positions using a thickness gauge that modified for measurement on curve surface. The modification of the thickness gauge is illustrated in Figure 5-3. Image (a) and (b) shows the entire thickness gauge and gauge head before modifying respectively. Two hemisphere beads 3.5mm in diameter were attached on each side of gauge head using Loctite Super Glue (Loctite, Henkel Ltd, Cheshire, UK) to enable the thickness gauge to measure thickness more accurately on curve surface shown in image (c). In image (d), the dial window of the modified thickness gauge was set to zero prompt to measure a thickness of the AFO (Figure 5-4).

Figure 5-3 Thickness gauge modification

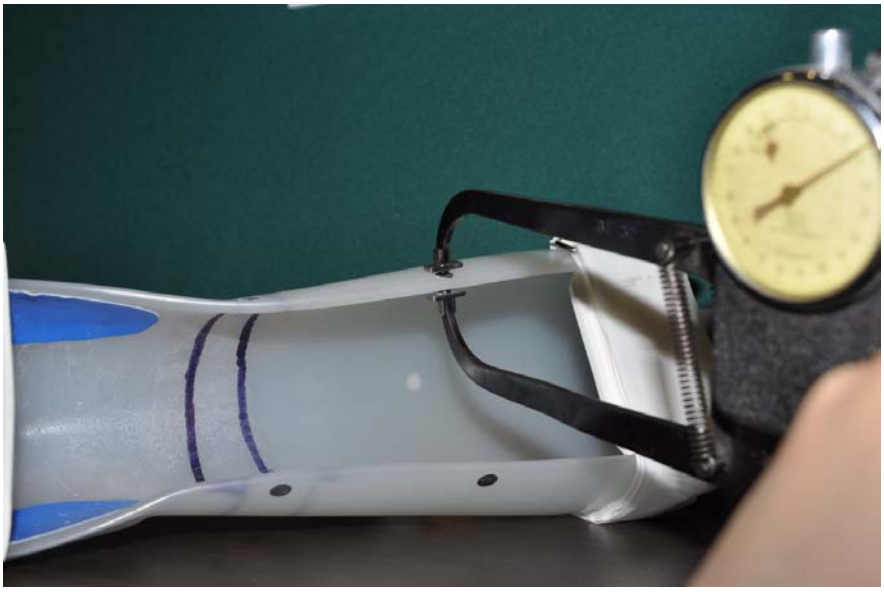

Figure 5-4 The AFO thickness measurement set up

The thickness at 33 positions marking on the AFO (Figure 5-5) was measured using the modified thickness gauge, and the measurement was taken five times at each position. The measurement results are shown in the Table 5-1 together with the average thickness and the standard deviation.

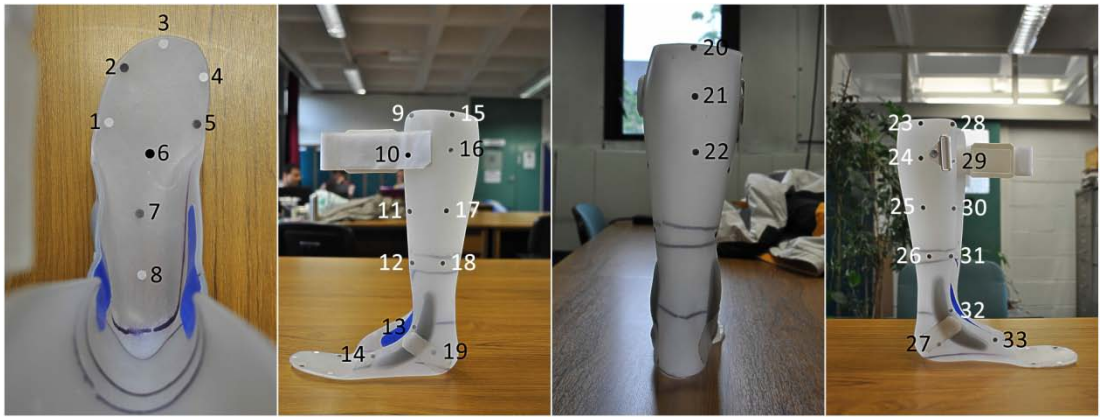

Figure 5-5 33 positions of the AFO thickness measurement

Measurement position	Thickness (mm)					
	1st measurement	2nd measurement	3rd measurement	4th measurement	5th measurement	Average
1	4.00	3.90	4.00	4.00	4.00	3.98 ± 0.04
2	4.00	3.90	4.00	3.90	4.00	3.96 ± 0.05
3	4.00	4.00	4.00	4.00	4.00	4.00 ± 0.00
4	3.80	3.80	3.90	3.90	3.90	3.86 ± 0.05
5	4.00	4.00	4.00	4.00	4.00	4.00 ± 0.00
6	3.80	3.80	3.80	3.80	3.80	3.80 ± 0.00
7	3.40	3.70	3.50	3.50	3.60	3.54 ± 0.11
8	2.50	2.60	2.40	2.50	2.50	2.50 ± 0.07
9	4.60	4.60	4.60	4.50	4.60	4.58 ± 0.04
10	4.20	4.20	4.20	4.20	4.30	4.22 ± 0.04
11	4.40	4.40	4.40	4.40	4.40	4.40 ± 0.00
12	4.20	4.20	4.20	4.20	4.20	4.20 ± 0.00
13	3.90	3.90	3.90	4.00	3.80	3.90 ± 0.07
14	4.50	4.50	4.50	4.50	4.40	4.48 ± 0.04
15	4.20	4.20	4.20	4.20	4.20	4.20 ± 0.00
16	4.00	4.00	4.00	4.00	4.00	4.00 ± 0.00
17	4.40	4.40	4.40	4.40	4.40	4.40 ± 0.00
18	4.40	4.40	4.50	4.40	4.50	4.44 ± 0.05
19	2.80	2.80	2.80	2.80	2.80	2.80 ± 0.00
20	4.20	4.20	4.10	4.10	4.20	4.16 ± 0.05
21	4.20	4.20	4.20	4.20	4.20	4.20 ± 0.00
22	4.50	4.50	4.40	4.60	4.50	4.50 ± 0.07
23	4.20	4.20	4.20	4.20	4.20	4.20 ± 0.00
24	4.30	4.20	4.20	4.20	4.30	4.24 ± 0.05
25	4.50	4.60	4.50	4.60	4.60	4.56 ± 0.05
26	4.80	4.80	4.80	4.80	4.80	4.80 ± 0.00
27	2.80	2.90	2.80	2.90	2.80	2.84 ± 0.05
28	4.20	4.20	4.30	4.30	4.30	4.26 ± 0.05
29	4.20	4.20	4.20	4.20	4.20	4.20 ± 0.00
30	4.50	4.50	4.50	4.50	4.50	4.50 ± 0.00
31	4.60	4.60	4.70	4.70	4.60	4.64 ± 0.05
32	4.30	4.40	4.30	4.30	4.30	4.32 ± 0.04
33	4.00	4.00	4.00	4.00	4.00	4.00 ± 0.00

Table 5-1 The AFO thickness measurement results with the average thickness and the standard deviation

In this study, the AFO FE models both constant and variable thickness were analysed using ANSYS software to compare to gain an accurate result. The constant thickness used in this study is 4.08mm obtained from the average of the values in the last column of Table 5-1, while the variable thickness gained from the average of the average thickness values in each region from eight regions of the AFO. The AFO thickness values were split into eight groups of thickness correspond to the location and the similarity of the thickness value. The locations of AFO thickness region and the average thickness of each region can be seen in the Figure 5-6 and the Table 5-2 respectively.

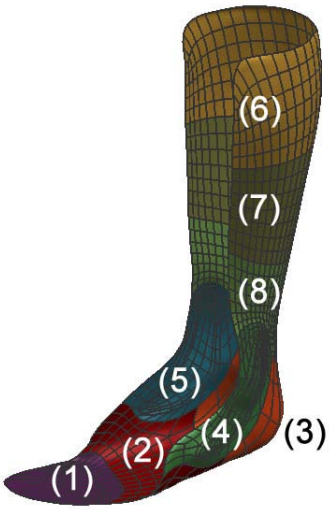

Figure 5-6 AFO split in to eight thickness regions

Measurement region	Average thickness (mm)
1 Metatarsal	3.96 ± 0.06
2 Midfoot	3.67 ± 0.18
3 Heel	2.71 ± 0.19
4 Lateral malleolus	4.19 ± 0.41
5 Medial malleolus	4.16 ± 0.23
6 Upper calf	4.23 ± 0.14
7 Central calf	4.47 ± 0.07
8 Lower calf	4.52 ± 0.26

Table 5-2 Average AFO thickness in each region

5.2.2 Mesh

Meshing method and mesh sensitivity study are clarified in this part.

5.2.2.1 Meshing method

A physics preference option used for meshing in this study allowed ANSYS 14.0 software to automatically performed meshing itself based on the physics of the analysis type specified. The suitable values in various meshing controls were set by the physics preference option, for example on: curvature, the value, chosen for use advanced size function, the meshing control, to appropriate with shell model analysis. However, a relevance option used to control the fineness of the mesh for the entire model was manually adjusted regarding the meshing time and the mesh quality (ANSYS 2011).

5.2.2.2 Mesh sensitivity study

A mesh sensitivity study could be used to indicate that the FEA model was sufficiently refined to assure the results were not dependent on the size of the finite element mesh. Eleven analyses were performed to study the sensitivity of the mesh. All conditions such as geometry and static structural in each analysis were similar except the mesh size. The relevance option was used to control the fineness of the mesh by adjust the range of value from -100 (high speed solution, coarser mesh, less accuracy) to +100 (slower speed solution, finer mesh, higher accuracy) at interval of 20 (ANSYS 2011). The solution called equivalent (von-Mises) stress used in the mesh sensitivity study to get a result, and the results from all analyses were then compared to define the appropriate mesh size. The analysis results are shown in the Table 5-3.

Analysis number	Mesh				Static structural analysis	Analysis time (min)
	Relevance	Max face size (mm)	Nodes	Elements	Equivalent (von-Mises) stress (MPa)	
					Maximum	
1	-100	2.6288	38259	38343	455.81	4
2	-80	2.3133	46099	46109	459.31	5
3	-60	2.0241	33920	33966	455.75	3
4	-40	1.7613	43383	43385	461.61	3
5	-20	1.5247	131165	130999	466.63	13
6	0	1.3144	n/a	n/a	n/a	n/a
7	20	1.1304	131165	130999	466.63	11
8	40	0.97264	131198	131058	466.63	9
9	60	0.8412	173543	173628	475.72	16
10	80	0.73605	n/a	n/a	n/a	n/a
11	100	0.65719	n/a	n/a	n/a	n/a

Table 5-3 The analysis results of mesh sensitivity study

Three analyses: analysis number 6, 10, and 11 could not perform meshing due to an error in meshing process in ANSYS software. As can be seen, the results of analysis number 5, 7, and 8 using relevance -20, 20, and 40 respectively were similar. The mesh generated in the analysis number 8 was the finest mesh among three mesh sizes in these analyses. The analysis time used in these three analyses was reasonable and not much different. The finer the mesh generated, the more accurate the result gained. However, a finer mesh used more elements, more time, and ultimately, more system resources. Therefore, the relevance value 40 was chosen to control the fineness of the mesh in the further analyses in this study regarding the mesh quality and the meshing time.

5.2.3 Static structural analysis

Analysis settings, loads, constraints, and solutions are explained in this section.

5.2.3.1 Analysis settings

A static analysis could be either linear or nonlinear. Nonlinear structural behavior arose from a number of causes such as geometric nonlinearities and material nonlinearities. In this analysis, the material nonlinearities were unlikely to be cause of nonlinear structural behavior due to the linear stress-strain relationship illustrated in Figure 5-2. To perform nonlinear analysis affected by the material nonlinearities, the multilinear elasticity gained from the tensile test was necessary. However, the

geometric nonlinearities, the AFO experiences large deformations, might be cause of nonlinear structural behavior in this analysis. Therefore, both linear and nonlinear analyses were chosen to predict the effect of loads on the AFO. To perform nonlinear analysis due to geometric nonlinearities, a solution option called large deflection in the analysis settings needed to be activated (Syngellakis, Arnold et al. 2000; ANSYS 2011).

5.2.3.2 Loads

An FEA in this study represented the AFO during heel off phase. Heel off phase was chosen as an interested gait component to analyse because the largest internal ankle joint moment and ankle joint power were generated during this phase (Whittle 2007). All loads detected at approximate 50% of gait cycle gained from the experiment were applied on the FE model in the same magnitudes and positions in ANSYS software for further analysis.

The average pressures at all sensor positions during heel off obtained from the F-Scan system experiment were located on the FE model in the Figure 5-7 identified as follows: (1) lateral metatarsal, (2) medial metatarsal, (3) lateral midfoot, (4) medial midfoot, (5) lateral heel, (6) medial heel, (7) upper central calf, (8) central central calf, (9) lower central calf, (10) upper lateral calf, (11) central lateral calf, (12) lower lateral calf, (13) upper medial calf, (14) central medial calf, (15) lower medial calf, (16) lateral ankle, (17) central ankle, and (18) medial ankle. The direction of these pressures was perpendicular to the AFO surface (Figure 5-8).

Figure 5-7 Locations of loads applied on FE model of AFO

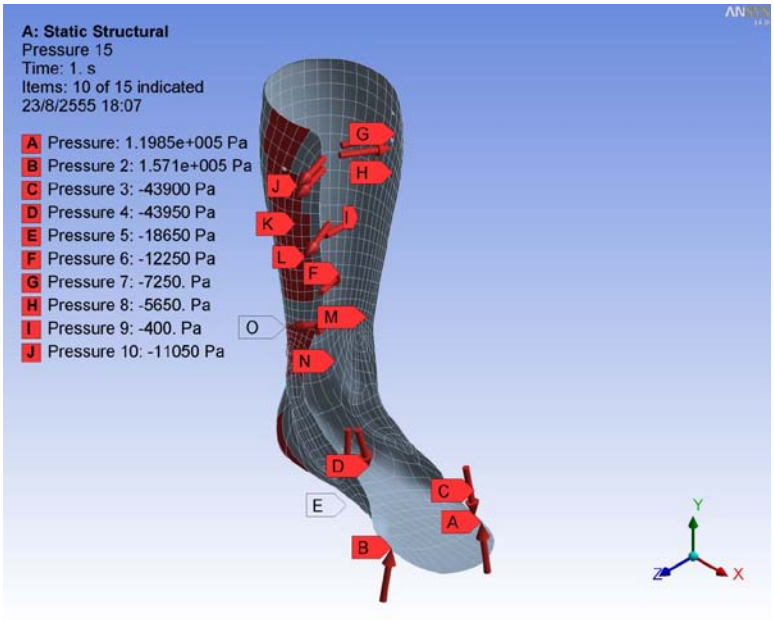

Figure 5-8 Directions and magnitudes of pressures applied on FE model of AFO

To apply the forces at lower and upper strap positions ((19) and (20) in Figure 5-7), the results, the plots of force versus frames, from the F-Scan system experiment were necessary. The plot of the force applied on the lower strap (Figure 5-9) could be obtained from the previous experiment, while another experiment needed to quantify the force acted on the upper strap.

The model 9811 sensor was attached to the upper strap by double sided tape for the experiment measuring force applied to this area. However, the model 3000 sensor was needed for this experiment as well to define the frame that interested gait component located. Therefore, two sensors were used in the experiment to quantify the upper strap force (Figure 5-10). The measurement method was similar to the method done in the previous F-Scan system experiment. The result needed from this experiment was also the plot of force applied on the strap versus frames using F-Scan Research software for further analysis (Figure 5-11).

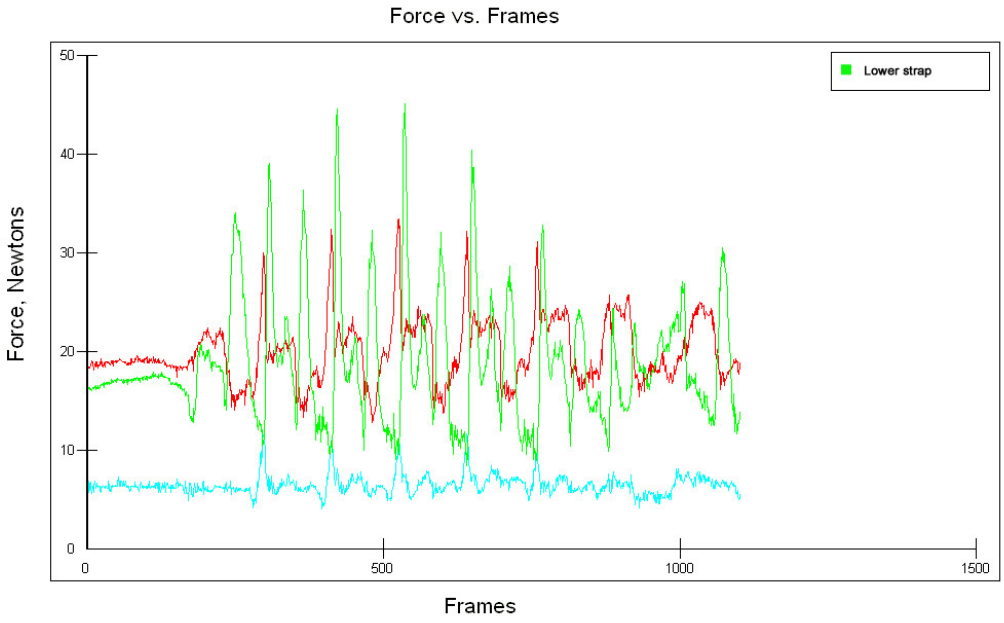

Figure 5-9 A plot of lower strap force versus frames

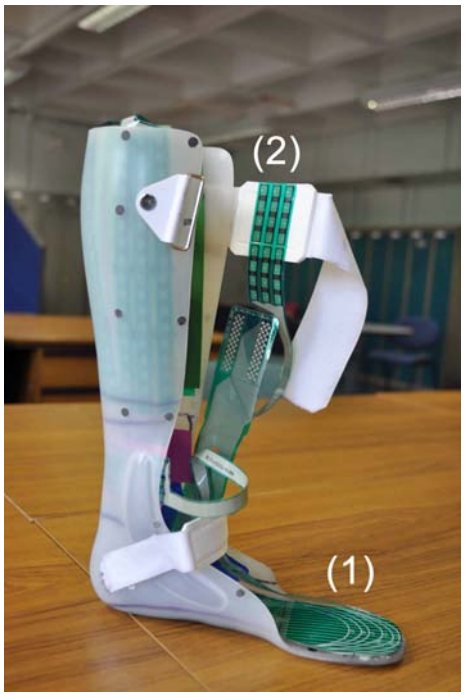

Figure 5-10 Sensor positions: (1) sole, (2) strap

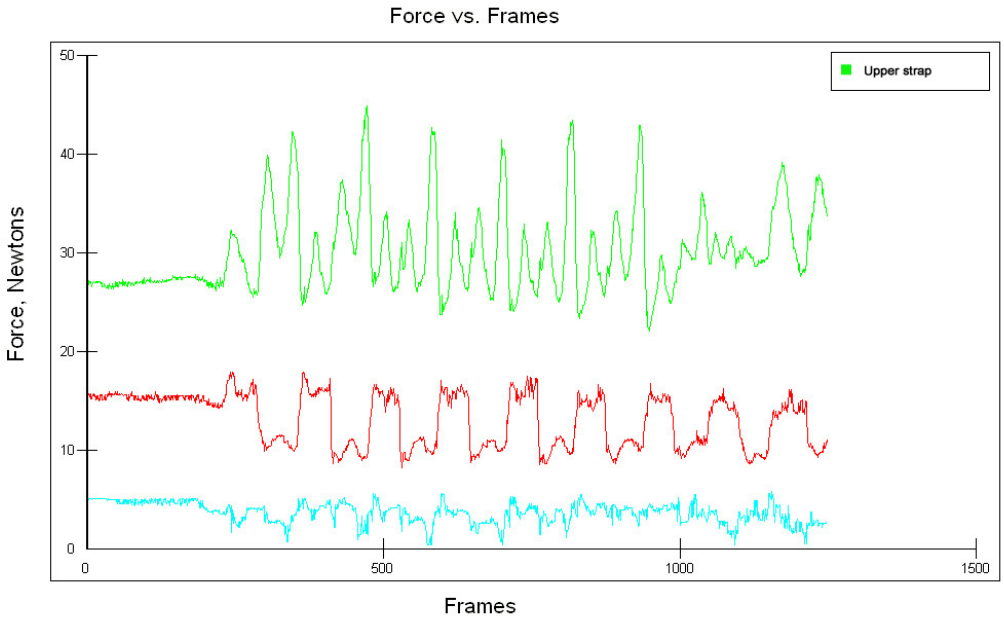

Figure 5-11 A plot of upper strap force versus frames

The results of strap force measurement were analysed and plotted regarding the gait components shown in Figure 5-12.

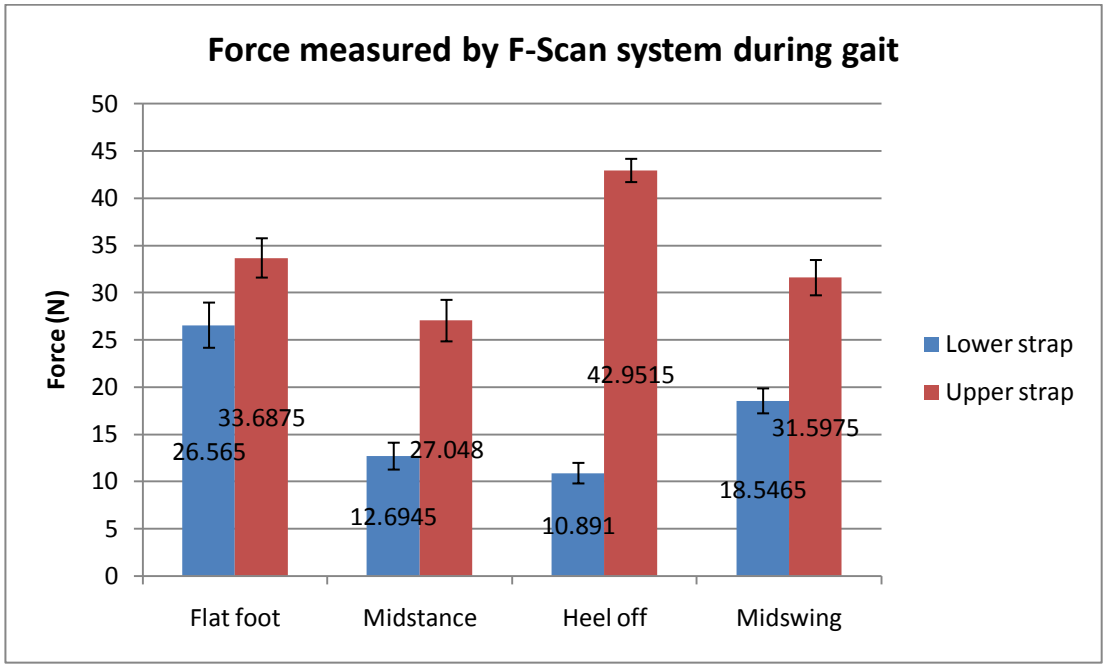

Figure 5-12 Plot of strap force measured by model 9811 sensor during gait

The total force at upper strap during heel off was divided into three forces to apply at three rivets fixing the strap, while the total force at lower strap was divided into two equal forces apply at two fixing areas. The directions and magnitudes of these forces are illustrated in Figure 5-13.

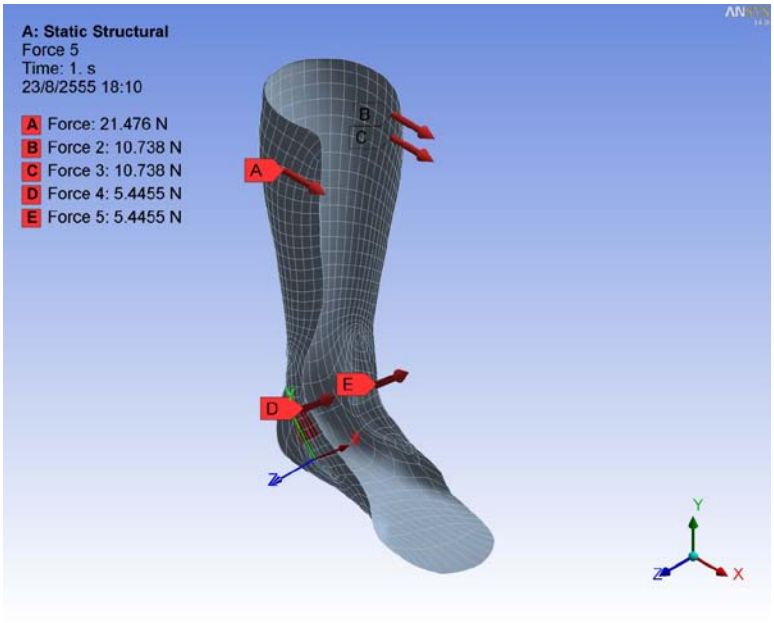

Figure 5-13 Directions and magnitudes of forces applied on FE model of AFO

5.2.3.3 Constraints

Two possible positions on AFO surface could be applied a constraint called fixed support, this constraint fixes both translation and rotation in all axes of the coordinate system, to fix a movement of AFO in ANSYS software that simulates the real condition of the AFO during heel off (Figure 5-14). One was the metatarsal area shown in image (a), and another one was the upper strap area shown in image (b). To clarify the real condition of the AFO during heel off, a normal gait performed by the subject was recorded as a video at 24 frames per second in frame rate. The recorded video was then extracted into a number of images at 24 images per one second of the video recording. The aim of using the images extracted from the video was to reveal the real condition of the AFO at each gait component. The appropriate images could be defined in term of gait component using the gait analysis theory in the literatures (Gage, Deluca et al. 1995; Whittle 2007). The extracted images were defined to four gait components: foot flat, midstance, heel off, and toe off detailed in

Figure 5-15. The two results obtained from two FEA using two different areas to apply constraint were used to validate an image that represents heel off phase. The constraint position in an analysis that simulates the most accurate real condition validating the image was chosen to use its condition in all further analyses in this study.

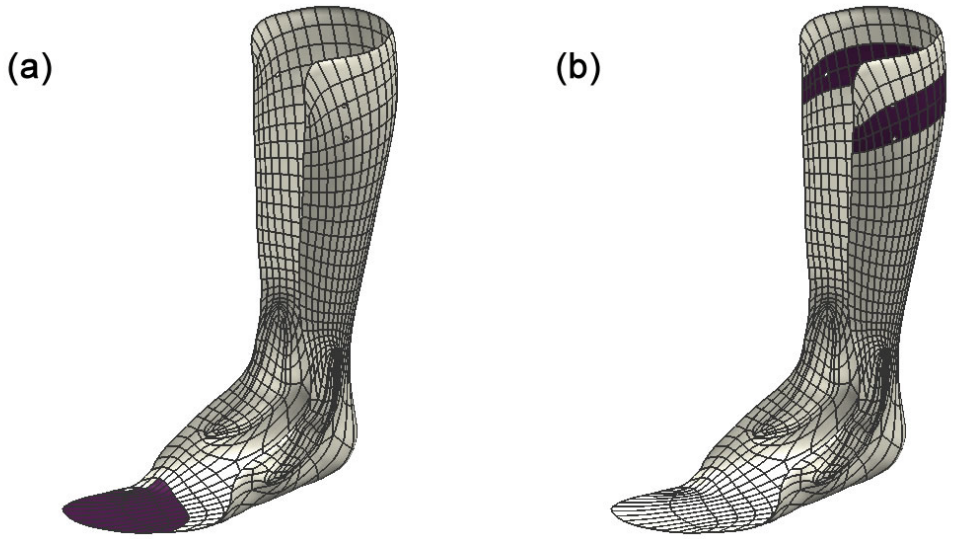

Figure 5-14 Two possible areas to apply constraint in FEA

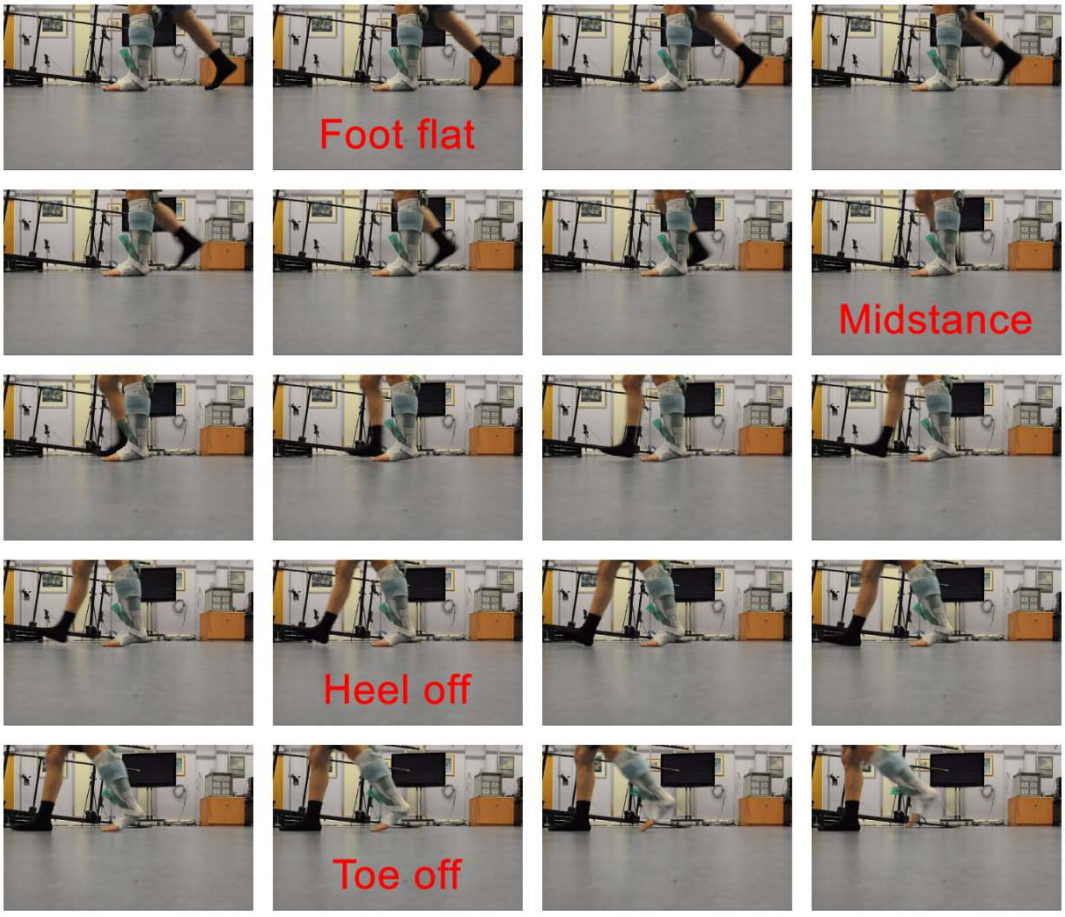

Figure 5-15 The images defined in term of gait components

The two simulation results, one gained from the new analysis number 12 that the constraint applied at the metatarsal area (image (b) in Figure 5-16), and another one obtained from the analysis number 8 applying the constraint at the upper strap area done in the mesh sensitivity study (image (b) in Figure 5-17), were validated the image that represent the heel of phase (image (a) in Figure 5-16 and 5-17). The validation can be seen in Figure 5-16 and Figure 5-17.

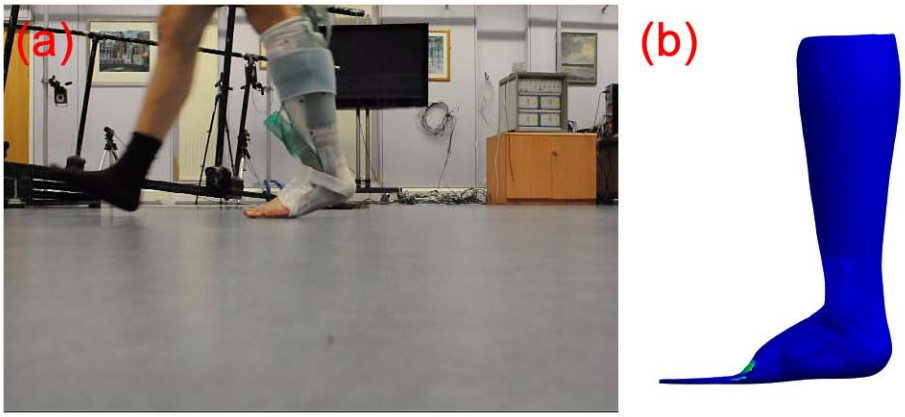

Figure 5-16 The simulation in analysis number 12 validated the image represented heel off

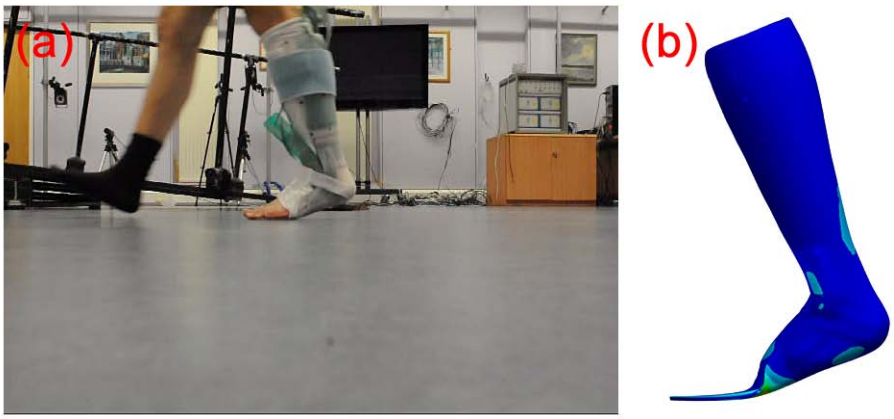

Figure 5-17 The simulation in analysis number 8 validated the image represented heel off

As can be seen, the deformation of the AFO affected by loads applied simulating in the analysis number 8 was more accurately than the simulation in the analysis number 12 validated to the image that represents the real condition of the AFO during heel off phase. Therefore, the constraint called fixed support using in the further analysis was then applied in the upper strap area.

5.2.3.4 Solutions

In this study, both linear and nonlinear static structural analyses were performed to discover the solution obtaining the most accurate result to validate a real-world

experiment. The details of four analyses performed in this study are shown in Table 5-4.

Analysis number	Geometry	Mesh			
	Thickness	Relevance	Max face size (mm)	Nodes	Elements
8	Constant	40	0.97264	131198	131058
13	Variable	40	0.97264	131198	131058
14	Constant	40	0.97264	131198	131058
15	Variable	40	0.97264	131198	131058

Table 5-4 The details of four analyses

Analysis number	Static structural analysis			
	Analysis settings	Forces	Pressures	Constraints
	Large deflection			
8	Inactivated	Obtained from Tekscan sensor		Fixed at calf strap
13	Inactivated	Obtained from Tekscan sensor		Fixed at calf strap
14	Activated	Obtained from Tekscan sensor		Fixed at calf strap
15	Activated	Obtained from Tekscan sensor		Fixed at calf strap

Table 5-4 The details of four analyses (Continued)

The solutions were used in each analysis to gain the interested outputs for further validation identified as follows:

- Equivalent elastic strain
- Maximum principal elastic strain
- Equivalent (von Mises) stress
- Maximum principal stress
- Strain probe
- Force reaction
- Moment reaction.

From elasticity theory, an infinitesimal volume of material at an arbitrary point on or inside the solid body can be rotated such that only normal stresses remain and all shear stresses are zero. The three normal stresses that remain are called the

principal stresses: maximum, middle, and minimum principal stresses. This principle can be used to define the principal strains as well. The equivalent stress, also called von Mises stress, related to the principal stresses is often used in design work because it allows any arbitrary three-dimensional stress state to be represented as a single positive stress value. Equivalent stress is part of the maximum equivalent stress failure theory used to predict yielding in ductile material. Poisson's ratio is necessary to compute equivalent elastic strain unlike equivalent stress computation (ANSYS 2011). Probes allow finding results at a point on the model. A strain probe, a force reaction probe, and a moment reaction probe were used in this study to find a strain in posterior ankle region at 86.16mm in height from the bottom surface of the AFO (Figure 5-18), reaction forces, and reaction moments at ankle joint respectively.

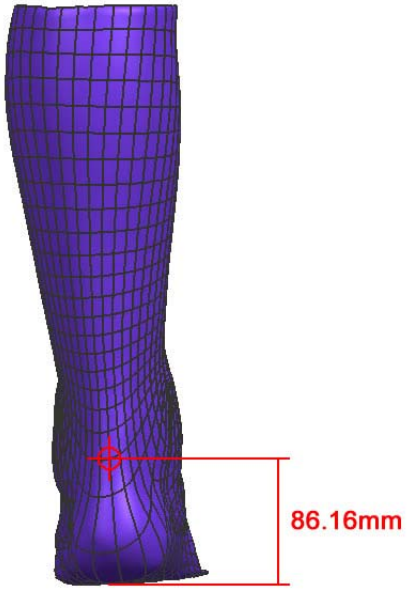

Figure 5-18 Strain probe position

5.2.4 Validation

To validate the analytical result obtained from the strain probe, the strain value gained from the corresponding real-world experiment was required. An experiment

to quantify the strain value in posterior ankle region of the AFO was perform using another existing similar homopolymer polypropylene AFO with 45° rectangular single-plane rosette strain gauge (Vishay Precision Group Inc, North Carolina, USA) installed in posterior ankle region at 75.00mm in height from the bottom surface of the AFO (Figure 5-19) that had previously been used in the experiment of Enrica Papi.

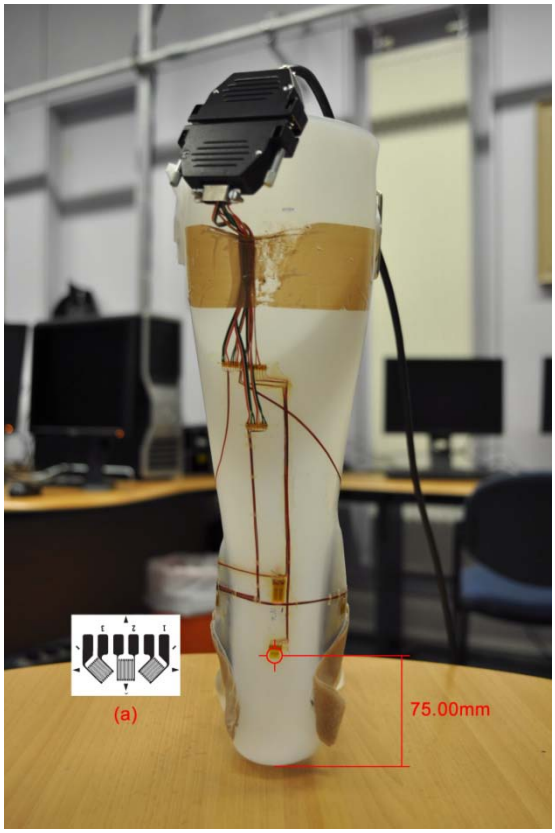

Figure 5-19 Homopolymer polrpropylene AFO with 45° rectangular single-plane rosette strain gauge (a) installed in posterior ankle region at 75.00mm in height from the bottom surface

The strain gauge was connected to the electrical components: Wheatstone bridge, amplifier, and analog-to-digital convertor wiring to the desktop computer which Vicon Nexus 1.8.2 software (Vicon Motion Systems Ltd, Oxford, UK) already exists to collect and process the output voltage gained from the strain gauge. The output voltage were collected at a sampling frequency 1000Hz as the subject walked with a normal gait for approximately seven gait cycles, and this was repeated twelve time. After processing, the collected data were then exported as ASCII data to Microsoft

Office Excel 2007 to analysis later. The strain value was calculated from output voltage using an equation identified as follow.

$$\varepsilon_0 = \frac{4e_0}{EK_SG}$$

Where ε_0 is a strain (mm/mm), e_0 is an output voltage (V), E is a bridge voltage (V), K_S is a gauge factor, and G is an amplifier gain. The bridge voltage 2V, the gauge factor 1.985, and the amplifier gain 500 were used in this experiment. The calculated strain data were divided into individual gait cycles based on the plot of the strain against the time (Figure 5-20) to quantify the strain value generated at approximate 50% of gait cycle that represents the heel off (Figure 5-21).

The maximum strain value during heel off calculated from the output voltage obtained from this experiment was a tensile strain 0.002482599496mm/mm or 2482.599496 microstrain. This value would be used to validate the analytical result gained from the strain probe.

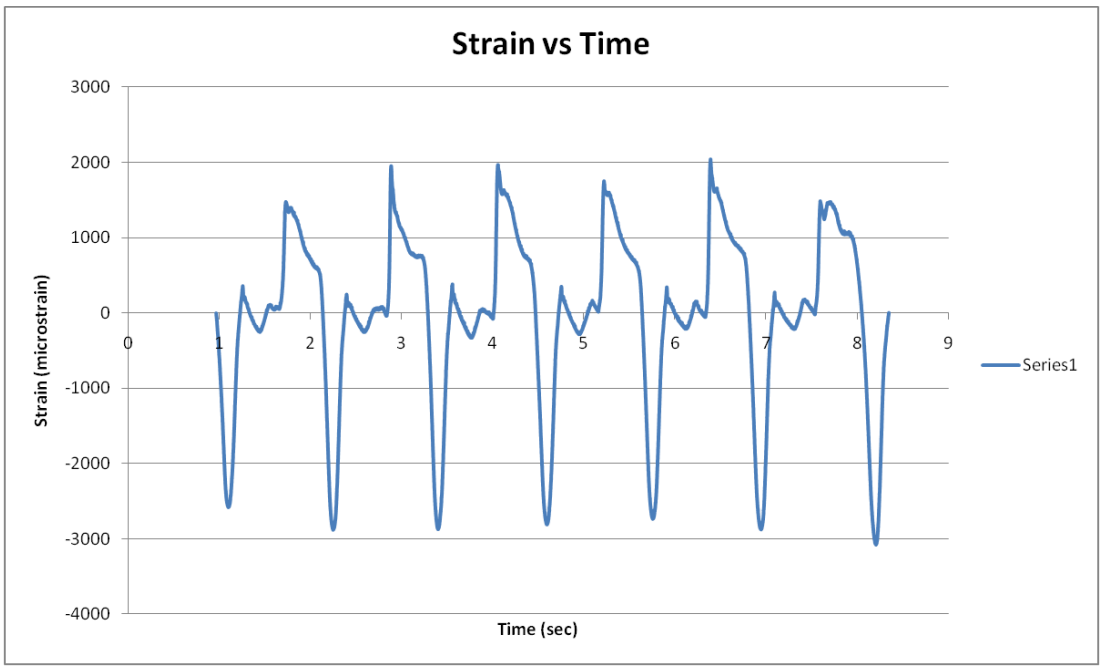

Figure 5-20 Plot of calculated strain data against time

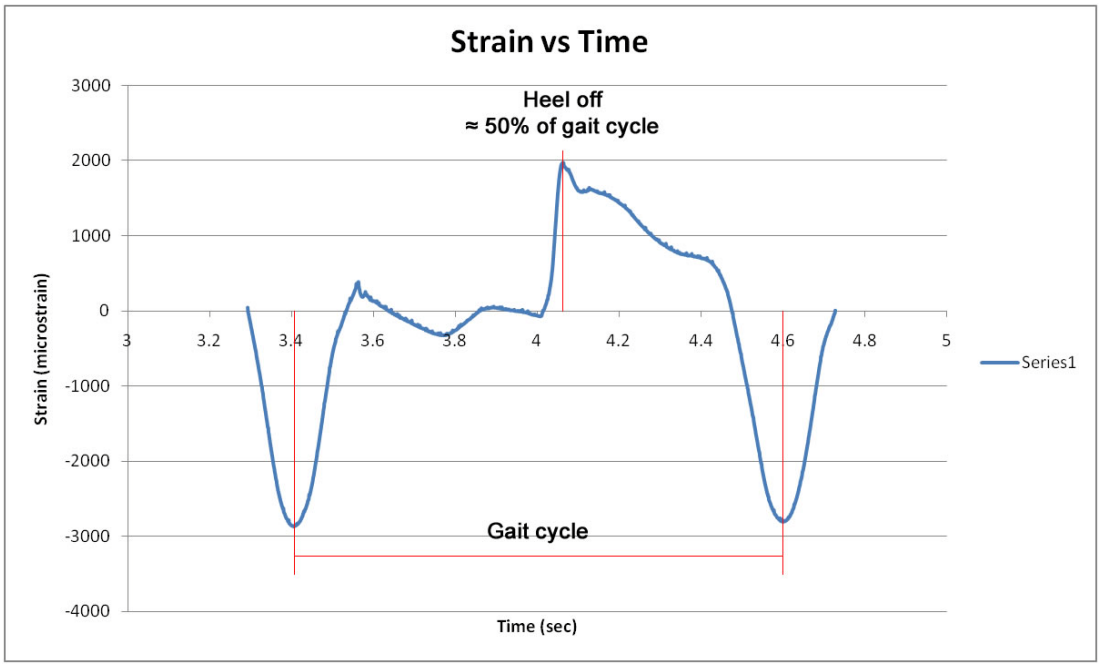

Figure 5-21 Plot of calculated strain data against time in one gait cycle shows the tensile strain generated during heel off

5.3 Results

All analytical results: stresses, strains, and loads are reported in Table 5-5, and samples of graphics image illustrating the analytical result gained from ANSYS software are shown in Figure 5-22 and Figure 5-23. Two analyses performing linear analysis were achieved, while another two analyses performing nonlinear analysis were failed due to solver in ANSYS software was unable to converge on a solution for the nonlinear problem as constrained. Refer to a clarification in ANSYS 14.0 Help, a nonlinear analysis might fail to converge due to a number of reasons such as large deformations that distort the mesh resulting in element shape errors, material instabilities, large load increments, and initially open contact surfaces causing rigid body motion. Although the analyses were restarted several times to recover from a convergence failure in the nonlinear analysis following a suggestion in ANSYS 14.0 Help, the error in convergence of the results still could not be solved. Therefore, there are only the results obtained from the two linear analyses, analysis number 8 and number 13 available for further validation in this study.

Analysis number	Static structural analysis				
	Solution				
	Equivalent elastic strain (mm/mm)	Maximum principal elastic strain (mm/mm)	Equivalent (von Mises) stress (MPa)	Maximum principal stress (MPa)	Strain probe (mm/mm)
	Maximum	Maximum	Maximum	Maximum	Normal Y Axis
8	0.22797	0.10744	466.63	208.3	0.0088173
13	0.2594	0.12248	530.99	225.65	0.010547
14	n/a	n/a	n/a	n/a	n/a
15	n/a	n/a	n/a	n/a	n/a

Table 5-5 The results of four analyses

Analysis number	Static structural analysis					
	Solution					
	Force reaction (N)			Moment reaction (N.m)		
	Normal X Axis	Normal Y Axis	Normal Z Axis	Normal X Axis	Normal Y Axis	Normal Z Axis
8	156.6	-770.8	71.658	48.813	-1.6328	-147.98
13	156.6	-770.8	71.658	48.813	-1.6328	-147.98
14	n/a	n/a	n/a	n/a	n/a	n/a
15	n/a	n/a	n/a	n/a	n/a	n/a

Table 5-5 The results of four analyses (Continued)

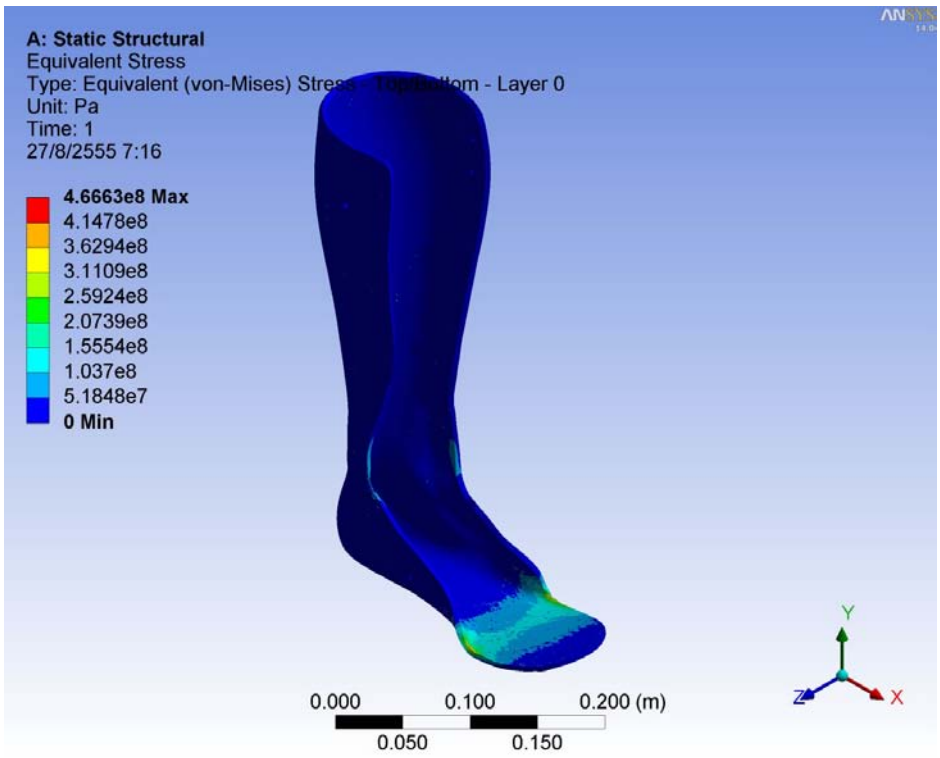

Figure 5-22 Graphics image of von Mises stress distribution in AFO in analysis number 8

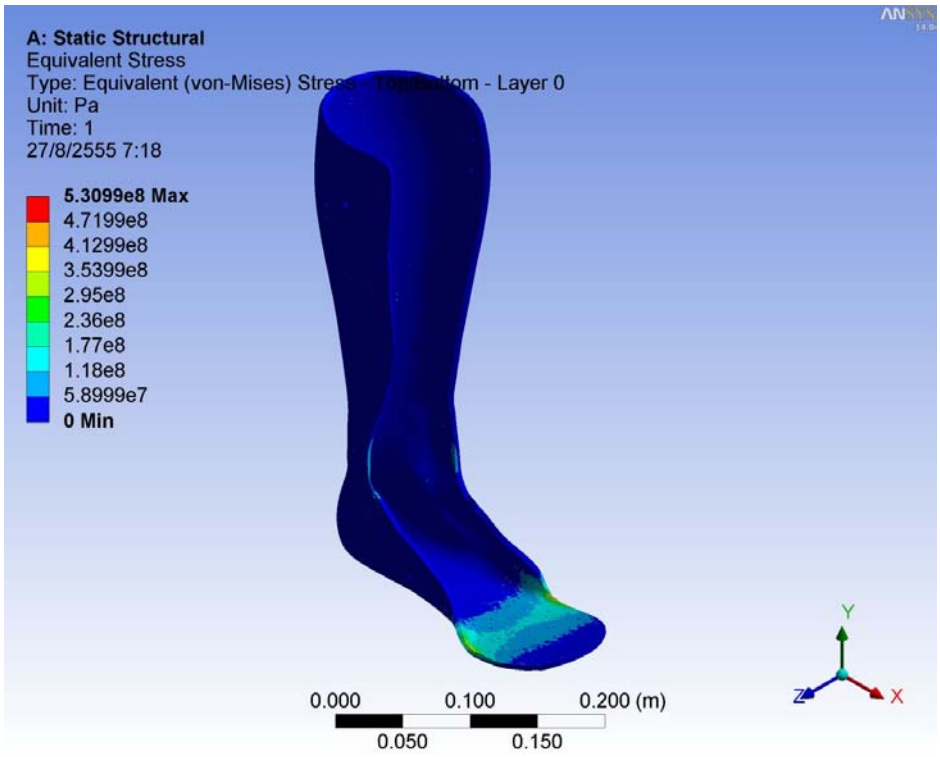

Figure 5-23 Graphics image of von Mises stress distribution in AFO in analysis number 13

Due to the failure of nonlinear analysis, there was only two analytical data left to compare among themselves. Only one difference between FE model in analysis number 8 and number 13 was thickness. The thickness used for FE model in analysis number 8 was a constant thickness 4.08mm throughout, while in analysis number 13 was a variable thickness. Therefore, only the effect of thickness on analytical result could be compared. All analytical results except reaction loads in analysis number 13 were greater than the results in analysis number 8. The results of equivalent elastic strain, maximum principal elastic strain, von Mises stress, maximum principal stress, and strain probe in analysis number 13 were 13.787%, 13.999%, 13.793%, 8.329%, and 19.617% respectively larger than the results in analysis number 8. This could be only concluded that the difference between uniform and variable thickness of FE model might have significant effect on the analytical data. However, the comparison of the accuracy between the results of the analysis using constant and variable thickness FE model could not be justified until validated by corresponding experimental results.

The experiments and analyses similar to the experiments and the analyses done in this study were performed in a study by Henderson (Henderson 2011). Moreover, the same AFO used by Henderson was also used in this study. Therefore, the corresponding experimental results quantified in the study by Henderson could be possibly used to validate the results in this study as well. A result of strain measured in posterior ankle region at 75.00mm in height from the bottom surface of the AFO in the experiment done by Solomonidis et al. mentioned in the study by Henderson was -2310 microstrain or compressive strain 0.00231mm/mm definitely different from the analytical results of strain probe in this study were tensile strain 0.0088173mm/mm and 0.010547mm/mm obtained from the analysis number 8 and 13 respectively. Although the strain in this study measured in posterior ankle region at 86.16mm in height from the bottom surface of the AFO different from the measurement position mention in the study of Henderson, both results should not have been much different due to both measurement position located closely in the same region. However, a study of Feng and the studies of Chu et al. revealed that the stress generated at the neck of AFO during toe off was tensile stress (Chu and Reddy 1995; Chu, Reddy et al. 1995; Feng 1997; Chu and Feng 1998). This could be implied that the strain measured in the posterior ankle region during heel off would be tensile strain. Subsequently, the experiment measuring the strain value similar to the one done by Solomonidis et al. was performed. The result

2482.599496 microstrain or tensile strain 0.002482599496mm/mm obtained from this experiment was 28.16% and 23.54% as large as the analytical strain result gained from analysis number 8 and 13 respectively.

Furthermore, a force platform experiment performed by Solomonidis et al. using the same AFO and subject that also used in this study was mentioned in the study of Henderson as well. The experiment of Solomonidis et al. reported the ground reaction force in Y axis was 827.86N and the reaction moment at ankle joint Z axis was dorsiflexion 120.41N.m during heel off that useful for quantifying the loads experienced by the AFO. To calculate the force and moment carried by the AFO, the two equations identified as follows were necessary.

$$F_{Total} = F_{Anatomical} + F_{Orthosis}$$

$$M_{Total} = M_{Anatomical} + M_{Orthosis}$$

The analytical reaction force and moment representing the force 770.8N and moment 147.98N.m applied on the AFO by the anatomy were replaced with the anatomical force and moment in the two equations. The experimental force 827.86N and moment 120.41N.m quantified by Solomonidis et al. were then replaced with the total force and moment in the two equations as well. Consequently, the orthosis force 57.06N and moment -27.57N.m could be solved from the equations. The orthosis force in Y axis and moment in sagittal plane revealed that the AFO in this study carried the force 57.06N or 6.89% to assist, and generated moment in dorsiflexion direction 27.57N.m or 18.63% to resist walking ability in a healthy subject without pathological gait.

5.4 Discussion

Only two linear analytical results are insufficient to validate the practical results to perfectly identify the accuracy and the reliability of the data acquired from the FEA software. However, they can be used to clearly confirm the significant effect of different thickness between uniform and variable thickness on the FEA results. The obviously difference in value of the both analytical data discovered in the comparison indicated that the difference between uniform and variable thickness of FE model definitely affects the FEA results, while the differences between the analysed and experimental results found in the validation cannot be used to justify

the accuracy and reliability of the both analytical results due to these differences may also affected by some factors other than the inaccuracy and unreliability. To clearly confirm the accuracy and the reliability of the analytical result, the similarity in geometry and material properties between the 3D model and the real-world object of the AFO, and the suitability of the result obtained from the corresponding real-world experiment for validation are necessarily required. Although the 3D model used in this analysis is constructed from the scanning of the real-world object, there are some differences between them. Firstly, the slight difference in their outer surface may occur due to the error in the process of the constructing the 3D model from the scanning data. Secondly, the scattering of the thickness values in the 3D model is quite neat on either constant or variable thickness, while there are no any patterns to definitely represent the scattered thickness values in the real-world object of the AFO due to it fabricated by the thermoforming process. Thirdly, the real-world AFO is reinforced by inserting of the two carbon fibers at the malleolus region in both lateral and medial side, but there are no any reinforcements added in the 3D model. Finally, there is a difference in their material properties, for example the Young's modulus used in this analysis is a constant value representing linearity of stress-strain curve, while the actual relationship of stress-strain of the homopolymer polypropylene is nonlinearity. Although a corresponding real-world experiment is conducted to quantify the result for validation, the analytical result is not perfectly validated due to some limitations. One is inadequate a variety of the analytical results for comparison. There are only analytical results obtained from the two linear analyses because the two nonlinear analyses due to geometric nonlinearities are unsuccessfully solved. Another one is inadequate experimental data for validation. Only one strain value measured at the slightly different position in posterior ankle region of the AFO is gained from the real-world experiment for validation. Moreover, the AFO used in strain measurement experiment is not the same AFO used in other experiments in this study. These are the factors making the outcome of the analysis cannot be adequately used to definitely justify the accuracy and the reliability of the FEA result in this study.

The nonlinear analyses caused by both of material nonlinearities and geometric nonlinearities are not successful in this study due to lack of nonlinear stress-strain curve and error in FEA software respectively. These analyses need to be achieved to obtain a various analytical results either to compare among analytical results or to validate experimental results effectively. To achieve the nonlinear analyses, the

multilinear elasticity of the homopolymer polypropylene gained from the tensile test and the solution to eliminate error in convergence of the results are necessarily required.

Nevertheless, the available linear analytical results are validated by the corresponding experimental results to confirm the accuracy and reliability of using FEA software to predict the effects of loads on the model. The analytical results of strain probe in this study are compared to the experimental result of strain measurement in the similar region on the AFO that mention in the previous study of Henderson revealing both results were definitely different. The result mentioned in the study of Henderson is compressive strain, while the two results in this study are tensile strain. However, there are findings in some literatures can be implied to use to support that the strain in this area is tensile strain. Subsequently, the experiment using strain gauge to measure the strain in the area corresponding to the analysis is conducted for more accurate and reliable confirmation. The strain value obtained from the experiment is only 28.16% and 23.54% as large as the analytical strain result gained from analysis number 8 and 13 respectively. These differences cannot be used to justify the accuracy and reliability of the both analytical results because a number of factors other than the inaccuracy and unreliability may also affect on them such as lack of reinforcement in 3D model, difference in geometry and material properties between 3D model and real-world AFO, and different AFO used in validation.

Furthermore, the analytical results in this study also illustrate that the AFO in this study experience the force only 6.89% of the overall magnitude of ground reaction force to assist, and generate moment in dorsiflexsion 18.63% of the overall magnitude of the moment generated by plantarflexor to resist walking in healthy subject with no pathological gait. To investigate the effective characteristics of the AFO, the similar experiment needs to be performed again using a subject with pathological gait for comparison.

On the whole, to conclude all of studies in this chapter perfectly, there are three things left needing to be completed. Firstly, the multilinear elasticity of homopolymer polypropylene need to be quantified and error in convergence of the results need to be completely solved leading to achievement in nonlinear analysis. Secondly, the strain measurement experiments need to be repeated to gain more practical results in the other different positions to effectively validate the analytical results in this

study. Finally, the all similar experiments need to be repeated using a subject with pathological gait to compare the different changes in biomechanical characteristics of the AFO responding to the different subject.

Chapter 6 Conclusion

6.1 General conclusions

The aim of this thesis, to develop a validated FE model of an AFO which can be used to analyse the loads applied during gait, has been achieved by completing the specific objectives identified as follows:

- The pressures acting on an AFO during normal gait are successfully measured using two different pressure measurement systems
- The position and magnitude of the pressures acting on the AFO are calculated using the experimental data
- The accurate a 3D digital surface model of the AFO is captured using the 3D digitiser for further analysis using FEA software
- The FE model of the AFO is successfully developed and can be used to predict the stresses, strains, and loads acting on the AFO
- The FEA results are validated using a strain data from a real-world experiment
- The stresses, strains, and loads acting on the AFO are analysed using the FEA results.

In the pressure measurement experiment, trends of the results obtained from the two sensors: F-Scan and pedar system are similar; however, the magnitudes tend to be different.

In the 3D scanning, the more data the AFO is scanned, the more accuracy the 3D model is constructed. The 16 scanned data is adequate to construct the 3D model of the AFO finely due to an overlap area on each scan that can be used to confirm one another the correct shape of the subject. The powder is use to spray on the translucent surface of the AFO to improve the scanned data.

In the validation, the differences between analytical and experimental data cannot be used to justify the accuracy and reliability of the analytical results because a number of factors other than the inaccuracy and unreliability may also affect on them. Based on healthy subject with no pathological gait, this study reveals that, on the one hand, the AFO is able to assist walking by carrying 6.89% of the overall magnitude of ground reaction force. On the other hand, it resists walking by

generating 18.63% in dorsiflexion of the overall magnitude of the moment generated by plantarflexor.

6.2 Recommendations for further study

To improve the accuracy and the reliability of the results in this study, there are three things left needing to be completed.

Firstly, the tensile test of the homopolymer polypropylene needs to be performed to quantify multilinear elasticity to use in nonlinear analysis due to material nonlinearities and error in convergence of the results need to be completely solved leading to achievement in nonlinear analysis due to geometric nonlinearities.

Secondly, the strain measurement experiments need to be repeated to gain more practical results in the other different positions to adequately and effectively validate the analytical results.

Finally, the all similar experiments need to be repeated using a subject with pathological gait to compare the different changes in biomechanical characteristics of the AFO responding to the different subject.

References

ANSYS (2011). ANSYS 14.0 Help, ANSYS, Inc.

Balaban, B., rol, et al. (2007). "The effect of hinged ankle-foot orthosis on gait and energy expenditure in spastic hemiplegic cerebral palsy." Disability and Rehabilitation **29**(2): 139-144.

Bregman, D. J. J., V. De Groot, et al. (2010). "Polypropylene Ankle Foot Orthoses to Overcome Drop-Foot Gait in Central Neurological Patients: A Mechanical and Functional Evaluation." Prosthetics and Orthotics International **34**(3): 293-304.

Bregman, D. J. J., A. Rozumalski, et al. (2009). "A new method for evaluating ankle foot orthosis characteristics: BRUCE." Gait & posture **30**(2): 144-149.

Burtner, P. A., M. H. Woollacott, et al. (1999). "Stance balance control with orthoses in a group of children with spastic cerebral palsy." Developmental Medicine & Child Neurology **41**(11): 748-757.

Chen, C.-L., K.-T. Yeung, et al. (1999). "Anterior ankle-foot orthosis effects on postural stability in hemiplegic patients." Archives of Physical Medicine and Rehabilitation **80**(12): 1587-1592.

Chu, T.-M. and R. Feng (1998). "Determination of Stress Distribution In Various Ankle-Foot Orthoses: Experimental Stress Analysis." Journal of Phrosthetics and Orthotics **10**(1): 11-16.

Chu, T.-M. and N. P. Reddy (1995). "Stress distribution in the ankle-foot orthosis used to correct pathological gait." Journal of Rehabilitation Research and Development **32**(4): 349-360.

Chu, T. M., N. P. Reddy, et al. (1995). "Three-dimensional finite element stress analysis of the polypropylene, ankle-foot orthosis: static analysis." Medical Engineering & Physics **17**(5): 372-379.

Cuccurullo, S. (2004). Physical medicine and rehabilitation board review. New York, N.Y., Demos.

de Wit, D. C., J. H. Buurke, et al. (2004). "The effect of an ankle-foot orthosis on walking ability in chronic stroke patients: a randomized controlled trial." Clinical Rehabilitation **18**(5): 550-557.

Edelstein, J. E. and J. Bruckner (2002). Orthotics : a comprehensive clinical approach. Thorofare, NJ, Slack.

Feng, R. (1997). Determination and studying of stress distribution in various ankle-foot orthoses: Experimental stress analysis. Biomedical Engineering. New Jersey, New Jersey Institute of Technology. **Master of Science**.

Gage, J. R., P. A. Deluca, et al. (1995). "Gait Analysis: Principles and Applications." The Journal of Bone & Joint Surgery **77**(10): 1607-1623.

Geomagic (2008). INTERACTIVE USER GUIDE Four Basic Workflows for Studio 10, Geomagic, Inc.

Gök, H., A. Küçükdeveci, et al. (2003). "Effects of ankle-foot orthoses on hemiparetic gait." Clinical Rehabilitation **17**(2): 137-139.

Henderson, G. (2011). Load analysis of ankle foot orthoses during gait. Bioengineering. Glasgow, University of Strathclyde. **Master of Science**.

Henderson, W. H. and L. W. Lamoreux (1969). "The orthotic prescription derived from a concept of basic orthotic functions." Bulletin of Prosthetics Research **6**(1): 89-96.

Hoppenfeld, S. and M. S. Zeide (1994). Orthopaedic dictionary. Philadelphia, J.B. Lippincott Co.

Hsu, J. D., J. W. Michael, et al. (2008). AAOS atlas of orthoses and assistive devices. St. Louis, Mo. ; London, Elsevier Mosby.

Hutton, D. V. (2004). Fundamentals of finite element analysis. Boston, McGraw-Hill.

INEOS (2010). Typical Engineering Properties of Polypropylene, INEOS Olefins & Polymers USA.

ISO (2003). ISO 8551:2003 Prosthetics and orthotics -- Functional deficiencies -- Description of the person to be treated with an orthosis, clinical objectives of treatment, and functional requirements of the orthosis. Geneva, Switzerland, International Organization for Standardization.

Kalamdani, A. A. (2006). Development and characterization of a high-spatial-temporal-resolution foot-sole-pressure measurement system. The Robotics Institute. Pennsylvania, Carnegie Mellon University. **Master of Science**.

Leone, D., S. Diemente, et al. (1988). Structural analysis of solid ankle-foot orthoses. Bioengineering Conference, 1988., Proceedings of the 1988 Fourteenth Annual Northeast.

Leung, J. and A. Moseley (2003). "Impact of Ankle-foot Orthoses on Gait and Leg Muscle Activity in Adults with Hemiplegia: Systematic literature review." Physiotherapy **89**(1): 39-55.

Lord, M. and D. Jones (1988). "Issues and themes in computer aided design for external prosthetics and orthotics." Journal of Biomedical Engineering **10**(6): 491-498.

Lucareli, P. R. G., M. d. O. Lima, et al. (2007). "Changes in joint kinematics in children with cerebral palsy while walking with and without a floor reaction ankle-foot orthosis." Clinics **62**: 63-68.

Lusardi, M. M. and C. C. Nielsen (2007). Orthotics and prosthetics in rehabilitation. St. Louis, Mo., Saunders/Elsevier.

McHugh, B. (1999). "Analysis of body-device interface forces in the sagittal plane for patients wearing ankle-foot orthoses." Prosthet Orthot Int **23**(1): 75-81.

Nakasone, Y., S. Yoshimoto, et al. (2006). Engineering analysis with ANSYS software. Amsterdam ; Boston, Butterworth-Heinemann.

Novel (2008). pedar®-x mobile pedography. N. GmbH. Munich, Novel GmbH.

Nowak, M. D., K. S. Abu-Hasaballah, et al. (2000). "Design enhancement of a solid ankle-foot orthosis: real-time contact pressures evaluation." J Rehabil Res Dev **37**(3): 273-281.

Ofir, R. and H. Sell (1980). "Orthoses and ambulation in hemiplegia: a ten year retrospective study." Archives of Physical Medicine and Rehabilitation **61**(5): 216-220.

Ounpuu, S., K. J. Bell, et al. (1996). "An Evaluation of the Posterior Leaf Spring Orthosis Using Joint Kinematics and Kinetics. [Miscellaneous Article]." Journal of Pediatric Orthopaedics **16**(3): 378-384.

Quesada, P. M., G. S. Rash, et al. (1997). "Assessment of pedar and F-scan revisited." Clinical Biomechanics **12**(3): S15.

Radtka, S. A., S. R. Skinner, et al. (1997). "A Comparison of Gait With Solid, Dynamic, and No Ankle-Foot Orthoses in Children With Spastic Cerebral Palsy." Physical Therapy **77**(4): 395-409.

Robin, G., A. Magora, et al. (1968). "Dynamic stress analysis of below-knee drop foot braces." Medical and Biological Engineering and Computing **6**(5): 533-546.

Shamp, J. A. K. (1983). "Ankle Foot Orthoses: Metal vs. Plastic." Clinical Prosthetics and Orthotics **7**(1): 1-3.

Sumiya, T., Y. Suzuki, et al. (1996). "Stiffness control in posterior-type plastic ankle-foot orthoses: Effect of ankle trimline Part 1: A device for measuring ankle moment." Prosthetics and Orthotics International **20**(2): 129-131.

Sumiya, T., Y. Suzuki, et al. (1996). "Stiffness control in posterior-type plastic ankle-foot orthoses: Effect of ankle trimline Part 2: Orthosis characteristics and orthosis/patient matching." Prosthetics and Orthotics International **20**(2): 132-137.

Svensson, W. and U. Holmberg (2010). "Estimating Ground Inclination Using Strain Sensors with Fourier Series Representation." Journal of Robotics **2010**.

Svensson, W., T. Salomonsson, et al. (2007). Foot orthosis strain sensing in hill walking. Rehabilitation Robotics, 2007. ICORR 2007. IEEE 10th International Conference on.

Syngellakis, S., M. A. Arnold, et al. (2000). "Assessment of the non-linear behaviour of plastic ankle foot orthoses by the finite element method." Proceedings of the Institution of Mechanical Engineers, Part H: Journal of Engineering in Medicine **214**(5): 527-539.

Tekscan (2006). F-Scan User Manual, Tekscan, Inc.

Tongbo, C., H. P. A. Lensch, et al. (2007). Polarization and Phase-Shifting for 3D Scanning of Translucent Objects. Computer Vision and Pattern Recognition, 2007. CVPR '07. IEEE Conference on.

Tyson, S. F. and H. A. Thornton (2001). "The effect of a hinged ankle foot orthosis on hemiplegic gait: objective measures and users' opinions." Clinical Rehabilitation **15**(1): 53-58.

Whittle, M. (2007). Gait analysis : an introduction. Edinburgh ; New York, Butterworth-Heinemann.

Woodburn, J. and P. S. Helliwell (1996). "Observations on the F-Scan in-shoe pressure measuring system." Clinical Biomechanics **11**(5): 301-304.

Yamamoto, S., S. Miyazaki, et al. (1993). "Quantification of the effect of the mechanical property of ankle-foot orthoses on hemiplegic gait." Gait & Posture **1**(1): 27-34.